Available online at www.sciencedirect.com
ScienceDirect
Geochimica et Cosmochimica Acta 73 (2009) 348–363
Geochimica et Cosmochimica Acta
www.elsevier.com/locate/gca

# Local coordination of Zn in hydroxy-interlayered minerals and implications for Zn retention in soils

Olivier Jacquat, Andreas Voegelin *, Ruben Kretzschmar

*Institute of Biogeochemistry and Pollutant Dynamics, Department of Environmental Sciences, ETH Zurich, CHN, CH-8092 Zurich, Switzerland*

Received 14 May 2008; accepted in revised form 27 October 2008; available online 5 November 2008

**Abstract**

The objective of this study was to determine the local coordination of Zn in hydroxy-interlayered smectite (HIS) as a function of Zn loading and synthesis conditions and to assess the importance of hydroxy-interlayered minerals (HIM) for Zn retention in contaminated soils. Published and newly collected extended X-ray absorption fine structure (EXAFS) spectra of HIS reacted with Zn at molar Zn/hydroxy-Al ratios from 0.013 to 0.087 (corresponding to final Zn contents of 1615–8600 mg/kg Zn) were evaluated by shell fitting. In Zn–HIS, Zn was octahedrally coordinated to oxygen at 2.06–2.08 Å and surrounded by Al atoms at 3.03–3.06 Å in the second-shell. With increasing molar Zn/hydroxy-Al ratio, the coordination number of second-shell Al decreased from 6.6 to 2.1. These results were interpreted as a progressive shift from Zn incorporation in the vacancies of gibbsitic Al-polymers to Zn adsorption to incomplete Al-polymers and finally uptake by cation exchange in the polymer-free interlayer space of HIS with increasing Zn loadings. In a second part, we determined the speciation of Zn in eight contaminated soils (251–1039 mg/kg Zn) with acidic to neutral pH (pH 4.1–6.9) using EXAFS spectroscopy. All soils contained hydroxy-Al interlayered vermiculite (HIV). The analysis of EXAFS spectra by linear combination fitting (LCF) showed that a substantial fraction of total Zn (29–84%) was contained in HIM with high Zn loading. The remaining Zn was adsorbed to organic and inorganic soil components and incorporated into phyllosilicates. In sequential extractions of Zn–HIS spiked into quartz powder and the Zn contaminated soils, Zn was mainly released in the two most resistant fractions, in qualitative agreement with the findings from LCF. Our results suggest that formation of Zn–HIM may strongly retain Zn in pristine and moderately contaminated acidic to neutral soils. Due to their limited sorption capacity, however, HIM do not allow for the accumulation of high levels of Zn in response to continued Zn input into soils.


## 1. INTRODUCTION

Hydroxy-interlayered minerals (HIM) are phyllosilicates containing hydroxy-polymers in their interlayer. They can form as a weathering product of chlorite or by the formation of hydroxy-polymers within the interlayers of smectite (HIS) and vermiculite (HIV) (Barnhisel and Bertsch, 1989). The positively charged hydroxy-polymers in the interlayer are either dioctahedral (gibbsitic) or trioctahedral (brucitic) island-type structures depending on the composing cations (Dixon and Jackson, 1962; Rich, 1968). Dioctahedral hydroxy-Al is the principal component of the non-exchangeable interlayer material in acidic soils, whereas trioctahedral hydroxy-Mg interlayering may be significant in marine sediments and alkaline soils (Rich, 1968). Moderately acidic soil pH, low organic matter content, oxidizing conditions and frequent wetting and drying are considered to favor the pedogenic formation of hydroxy-Al interlayered phyllosilicates (Rich, 1968).

The formation of hydroxy-Al interlayers in smectites or vermiculites strongly reduces the cation exchange capacity (CEC) and affects the ion sorption properties of the clay minerals (Barnhisel and Bertsch, 1989; Janssen et al., 2003b; Meunier, 2007). Laboratory studies have shown that Cu, Cd, Ni, Pb, and Zn sorb strongly to hydroxy-Al interlayered montmorillonite under acidic conditions, while

* Corresponding author. Fax: +41 44 633 11 18.
*E-mail address:* voegelin@env.ethz.ch (A. Voegelin).

0016-7037/$ - see front matter © 2008 Elsevier Ltd. All rights reserved.
doi:10.1016/j.gca.2008.10.026

adsorption to pure montmorillonite at acidic pH is dominated by cation exchange (Lothenbach et al., 1997; Saha et al., 2001; Janssen et al., 2003b). Furthermore, hydroxy-Al polymers bound to a clay surface have a higher affinity for metal sorption than pure Al hydroxides (Keizer and Bruggenwert, 1991). Recent studies on Zn sorption to hydroxy-interlayered minerals using extended X-ray absorption fine structure (EXAFS) spectroscopy confirmed the uptake of Ni and Zn into the vacant octahedral sites of gibbsitic hydroxy-Al interlayers in montmorillonite (Nachtegaal et al., 2005b; Schlegel and Manceau, 2007). Uptake of Zn into the vacant sites of gibbsitic sheets has also been documented for the phyllomanganate lithiophorite (Manceau et al., 2003; Manceau et al., 2005). In contrast, uptake of tetrahedrally or octahedrally coordinated Zn by pure gibbsite is mainly due to the formation of mononuclear bidentate sorption complexes (Roberts et al., 2003; Schlegel and Manceau, 2007).

The incorporation of Zn into the hydroxy-Al interlayers of HIM by specific adsorption may have a substantial impact on Zn bioavailability and mobility in acidic soils, where adsorption is otherwise mainly due to cation exchange (Scheinost et al., 2002; Janssen et al., 2003b). Using bulk- and μ-EXAFS spectroscopy, Zn incorporated into HIM (Zn–HIM) has so far been detected in one contaminated (Scheinost et al., 2002) and two uncontaminated acidic soils (Manceau et al., 2004; Manceau et al., 2005).

To date, the influence of the mode of Zn uptake (adsorption/coprecipitation) and of Zn loading on the local coordination of Zn in Zn–HIM has not been studied. Furthermore, data on the abundance of Zn–HIM in soils as a function of their physicochemical properties and on the importance of Zn–HIM for immobilization of Zn in soils is still lacking. The first objective of this study was to characterize the local coordination of Zn in a series of synthetic Zn–HIS in relation to synthesis conditions and Zn content. Based on these findings, the second objective was to determine the abundance and Zn-loading of Zn–HIM in a series of HIM-containing soils with different soil characteristics and variable level of Zn contamination using EXAFS spectroscopy. Finally, we aimed at relating Zn reactivity as inferred from batch and sequential extractions to molecular-level Zn speciation. For the purpose of this study, soils were sampled near galvanized power line towers. The soils differed in composition, but were all contaminated by aqueous Zn in the runoff water from the towers. This allows studying the effect of soil properties and Zn concentration on the formation of pedogenic Zn species without interference from primary Zn-bearing contaminants.

## 2. EXPERIMENTAL SECTION

### 2.1. Soil, samples and bulk soil properties

Eight topsoils (GER, MOM, SAR, CHI1, BUN, GRÜ, BIB2, HAU) developed from different parent materials were sampled across Switzerland close to the foundations of galvanized power line towers (Table 1). Runoff water containing aqueous Zn from the corrosion of the galvanized steel surfaces (Odnevall Wallinder et al., 2001) has led to local Zn contamination. The soils have developed from metamorphic (SAR), igneous (MOM, CHI) and sedimentary bedrocks (GER, BUN, GRÜ, BIB2, HAU). About 1 kg of the upper soil layer (0-5 cm) was collected at each site, air-dried at 25 °C, homogenized using an agate mortar and sieved to <2 mm. The dry samples were stored in plastic containers in the dark at room temperature. For analyses requiring powdered and homogenized material, an agate disc swing mill was used to prepare <50 μm powdered subsamples from the <2 mm soil material.

The soil pH was determined with a glass electrode in a suspension of 1 g of soil in 10 mL of 0.01 M $CaCl_2$ solution. Prior to measurement, the soil suspension was shaken for 10 minutes and equilibrated for at least 30 minutes. Total metal contents were quantified by analyzing pressed pellets (4 g powdered soil <50 μm and 0.9 g Licowax C®) with energy dispersive X-ray fluorescence (XRF) spectrometry (Spectro X-lab 2000). The exchangeable contents of Na, Mg, Al, K, Ca, Mn, and Fe were determined in duplicates by extracting 7 g of soil with 0.1 M $BaCl_2$ (prepared from doubly deionized water (DDI), 18.2 MΩcm, Milli-Q® Element, Millipore) at a solution-to-solid ratio (SSR) of 30 mL/g (Hendershot and Duquette, 1986). After centrifugation, the solutions were filtered (0.45 μm nylon filter, WICOM®) and acidified (1% (v/v) 30% $HNO_3$). The

Table 1
Physicochemical properties and Zn contents of the soil samples.

| Soil | Geology | pH ($CaCl_2$) | TOC (g/kg) | TIC (g/kg) | Texture (g/kg) | | | ECEC[a] ($mmol_c$/kg) | Total Zn (mg/kg) | Exch. Zn[b] (mg/kg (%)) |
|---|---|---|---|---|---|---|---|---|---|---|
| | | | | | Clay | Silt | Sand | | | |
| GER | Alluvium | 4.1 | 27 | — | 48 | 348 | 604 | 40 | 403 | 104 (26) |
| MOM | Paragneiss | 4.6 | 37 | — | 77 | 302 | 621 | 25 | 1039 | 286 (28) |
| SAR | Schist | 4.6 | 52 | — | 105 | 700 | 195 | 78 | 251 | 35 (14) |
| CHI1 | Orthogneiss | 4.9 | 14 | — | 42 | 149 | 809 | 4 | 971 | 118 (12) |
| BUN | Conglomerate | 5.5 | 44 | — | 215 | 455 | 330 | 149 | 852 | 139 (16) |
| GRÜ | Glacial till | 6.0 | 36 | 0.3 | 253 | 363 | 384 | 146 | 852 | 99 (12) |
| BIB2 | Conglomerate | 6.1 | 36 | 1.1 | 324 | 344 | 332 | 232 | 861 | 21 (2) |
| HAU | Limestone | 6.9 | 42 | 0.2 | 227 | 320 | 453 | 102 | 276 | <1 (<0.3) |

[a] Effective cation exchange capacity.
[b] Exchangeable Zn in 0.1 M $BaCl_2$ (SSR 30 mL/g; in parentheses percentage of total Zn).

extracts were analyzed by inductively coupled plasma-optical emission spectrometry (ICP-OES, Varian Vista-MPX). The effective cation exchange capacity (ECEC) was calculated from the charge equivalents of the extracted amounts of $Na^+$, $Mg^{2+}$, $Al^{3+}$, $K^+$, $Ca^{2+}$, and $Mn^{2+}$. Total carbon contents (TC) of powdered samples (<50 μm) were determined using a CHNS element analyzer (LECO CHNS-932). Total inorganic contents (TIC) of soils with pH >5.9 were determined by reacting 0.3–0.9 g of powdered soil <50 μm with 1 M $H_2SO_4$ in a reaction flask. The evolving $CO_2$ was trapped in a Nesbitt bulb containing NaOH-coated pellets and quantified gravimetrically. Total organic carbon contents were determined by subtracting the respective TIC content form the TC content. After pretreatment of the soil material <2 mm with $H_2O_2$ for removal of organic matter, the sand content (50–2000 μm) was quantified by wet sieving and the clay content (<2 μm) was determined using the pipette method (Gee and Or, 2002). The silt content (2–50 μm) of the soil samples was calculated to be the difference between the total soil weight and the sum of the sand and clay content (Gee and Or, 2002).

### 2.2. Clay extraction and analysis

To isolate the <2 μm size (clay) fraction, 20 g of soil were dispersed in 800 mL of 0.5 M NaCl. The suspension was subsequently sonified for 1 minute and passed through a 50 μm sieve. The sieved fraction > 50 μm was twice resuspended in DI water and sieved again to collect more fine material. The three bottles containing the filtrate were subsequentlyy centrifuged, the water decanted, and the sediment <50 μm resuspended and merged. After vigorous mixing of the suspension in a plastic bottle and allowing the settling of material > 2 μm (time calculated from Stoke's law), the top 10 cm of the 14 cm high water column were siphoned off. This procedure was repeated twice with fresh DI water to collect more clay (Kimpe, 1993b). The three clay suspensions were flocculated by $MgCl_2$ addition and merged. Excess salt was removed by three washing steps with DDI water until the supernatant was free of chloride ($AgNO_3$ test). The Mg-saturated clay was frozen in liquid $N_2$ (LN) and freeze-dried. K-saturated clay was prepared by exchanging 30 mg of Mg-saturated clay with 10 mL of 1.0 M KCl (Kimpe, 1993a). For complete exchange of the interlayer cations, the KCl solution was renewed twice. Excess salt was removed by three washing and centrifugation steps (5 min, 3400 g) using DDI water. Oriented specimens of the Mg- and K-saturated clay fractions were prepared by air-drying 30 mg of clay onto glass slides of 2.5 cm diameter. Ethylene glycol (EG) and glycerol (Gly) solvation was obtained by leaving an oriented Mg-saturated mount on the shelf of an EG or Gly-containing desiccator for 6 h at 60 °C and for 12 h at 110 °C, respectively (Brunton, 1955; Brown and Farrow, 1956). Oriented specimens of the citrate-extracted soil clay fraction (see Section 2.8 for details) were similarly prepared and analyzed. The K-saturated samples were placed for at least 1 h in a preheated muffle furnace at 100, 300 and 550 °C and measured by X-ray diffraction (XRD) after each heat treatment. X-ray diffraction patterns of the clay fractions were recorded on a Bruker D4 diffractometer equipped with a Cu anode and an energy dispersive SOL-X Si(Li) detector. Patterns were measured in continuous scan mode from 3° to 37° 2$\theta$ using variable slits, step size of 0.02° and a counting time of 4 s per step.

### 2.3. Reference compounds for EXAFS spectroscopy

In this study, we evaluated published and newly collected reference spectra for Zn-containing HIS, which differed in synthesis conditions (Table 2). All samples had in common that HIS was prepared by reacting Al with smectite (montmorillonite) at a ratio of 2 mmol/g. However, they differed in the duration of HIS aging (before/after Zn addition), mode of Zn incorporation (either coprecipitation during Al hydrolysis or sorption to preformed HIS), molar ratio of reacted Zn over hydroxy-Al ("Zn/Al ratio") and pH during Zn uptake (Table 2). Published EXAFS spectra for Zn–HIS synthesized by adsorbing Zn to preformed HIS at low Zn/Al ratios and near-neutral pH (Schlegel and Manceau, 2007) were kindly provided by Michel Schlegel (Commissariat à l'Énergie Atomique (CEA), Saclay, France). Briefly, HIS was synthesized from MX-80 montmorillonite (Clay Spur bed, Wyoming, USA; $N_2$-BET surface area of 31.3 $m^2$/g (Bradbury and Baeyens, 1998)). At pH 6.0 and 7.0, Zn–HIS was obtained by reacting 2 g/L of the HIS with 50 or 200 μM $ZnCl_2$, corresponding to Zn/Al ratios of 0.0125 and 0.05, respectively. After 1 d, the Zn–HIS were isolated ("Zn–HIS-1.6–pH 6", "Zn–HIS-1.6–pH 7", and "Zn–HIS-6.5–pH 7" in Table 2). Reference materials for Zn coprecipitated with Al during HIS formation were prepared in our laboratory at Zn/Al ratios of 0.2 and 0.5 at pH 4.5 and over a reaction period of 15 d ("Zn–HIS-7.6-CPT" and "Zn–HIS-7.7-CPT", respectively, in Table 2), as described in Scheinost et al. (2002). Also over a reaction time of 15 d, Zn was sorbed to preformed HIS at a Zn/Al ratio of 0.5 at pH 5.0 ("Zn–HIS-5.7-pH5" in Table 2). In order to prepare hydroxy-Al interlayered smectites with higher Zn/Al ratios (Zn/Al ratio between 1 and 25), a suspension of 20 g/L montmorillonite (SWy-2, Newcastle formation, Wyoming, USA, Clay Mineral Society Source Clays; $N_2$-BET surface area 31.8 $m^2$/g (van Olphen and Fripiat, 1979)) and 40 mmol/L $AlCl_3$ was slowly titrated to pH 4.5 with 0.1 M NaOH (Lothenbach et al., 1997). After equilibration for 15 h, the precipitate was washed four times with DDI water, frozen in LN and freeze-dried. Different loadings of Zn in HIS were obtained by suspending 1 g of HIS in 500 mL 10 mM $CaCl_2$ containing 2, 5, 10, 20 and 50 mM $ZnCl_2$, resulting in Zn/Al ratios of 1, 2.5, 5, 10, and 25, respectively (Table 2). The suspensions were aged during 15 h at pH 5.0. The final products were repeatedly washed with DDI water, frozen using LN and freeze-dried. The elemental composition determined by XRF showed that the fraction of Zn uptake decreased with increasing initial Zn/Al ratio, resulting in Zn contents of 2100 ("Zn–HIS-2.1-pH5"), 2900 ("Zn–HIS-2.9-pH5"), 4000 ("Zn–HIS-4.0-pH5"), 6900 ("Zn–HIS-6.9-pH5") and 8600 mg/kg ("Zn–HIS-8.6-pH5"). X-ray diffraction on oriented mounts of K-saturated Zn–HIS at increasing temperatures confirmed the formation of HIS.

Natural Zn-containing kaolinite ("natural Zn-kaolinite", 180 mg/kg Zn) from Decazeville, France and synthetic Zn-kaolinite ("synthetic Zn-kaolinite") were kindly provided by Farid Juillot (Institut de Minéralogie et de Physique des Milieux Condensés, Université Paris Diderot, Paris, France). The synthetic Zn-kaolinite was prepared as described in Petit et al. (1995). Briefly, 20 mL of 0.2 M ($Al(NO_3)_3 + Zn(NO_3)_2$) at Zn/Al ratio of 0.05 were added to 20 ml of 0.2 M $Na_2SiO_4 \cdot 5H_20$ and 20 ml 0.2 M NaOH under vigorous stirring during 1 h. The resulting gel was washed and centrifuged 3 times before drying at 80 °C during 48 h. 210 mg of the dried gel was dispersed in 30 mL DDI water and the suspension

Table 2
Synthesis conditions of Zn–HIS phases, product composition, and results from LCF (fits shown in Fig. EA2 electronic annex).

| Sample name | Synthesis conditions | | | | Product composition | | LCF results | | | |
|---|---|---|---|---|---|---|---|---|---|---|
| | pH | Initial[d] Zn/Al | Time[e] (d) | Uptake Mode[f] | Zn (mg/kg) | Final[g] Zn/Al | Zn-6Al[h] (%) | Zn-2Al[i] (%) | Zn–OS[j] (%) | NSSR (%) |
| Zn–HIS-1.6-pH6[a] | 6.0 | 0.013 | 1 | Ads | 1615 | 0.013 | — | — | — | — |
| Zn–HIS-1.6-pH7[a] | 7.0 | 0.013 | 1 | Ads | 1625 | 0.013 | 100 | — | — | 0.5 |
| Zn- HIS-6.5-pH7[a] | 7.0 | 0.05 | 1 | Ads | 6500 | 0.05 | 97 | — | — | 0.6 |
| Zn–HIS-7.6-CPT[b] | 4.5 | 0.2 | 15 | Cpt | 7600 | 0.067[g] | 78 | — | 15 | 2.9 |
| Zn–HIS-7.7-CPT[b] | 4.5 | 0.5 | 15 | Cpt | 7750 | 0.069[g] | 71 | — | 21 | 2.5 |
| Zn–HIS-2.1-pH5 | 5.0 | 1.0 | 0.63 | Ads | 2100 | 0.019[g] | 73 | — | 19 | 2.4 |
| Zn–HIS-2.9-pH5 | 5.0 | 2.5 | 0.63 | Ads | 2900 | 0.026[g] | 51 | 37 | 10 | 1.1 |
| Zn–HIS-4.0-pH5 | 5.0 | 5 | 0.63 | Ads | 4000 | 0.035[g] | 41 | 61 | — | 1.1 |
| Zn–HIS-5.7-pH5[b] | 5.0 | 0.5 | 15 | Ads | 5700 | 0.050[g] | 34 | 49 | 17 | 2.0 |
| Zn–HIS-6.9-pH5 | 5.0 | 10 | 0.63 | Ads | 6900 | 0.061[g] | 23 | 60 | 16 | 1.6 |
| Zn–HIS-8.6-pH5 | 5.0 | 25 | 0.63 | Ads | 8600 | 0.087[g] | 19 | 57 | 24 | 3.4 |
| Zn sorb. gibbsite-4.0 | 6.0 | — | — | Ads | 4000 | — | 5 | 80 | 8 | 1.7 |
| Zn sorb. gibbsite-1.9[c] | 6.0 | — | — | Ads | 1950 | — | — | — | | — |

[a] Spectra from Schlegel and Manceau (2007).
[b] Phases described in Scheinost et al. (2002).
[c] Spectrum from Roberts et al. (2003).
[d] Initial Zn/hydroxy-Al ratio during Zn uptake.
[e] Reaction time allowed for Zn uptake.
[f] Ads: Adsorption of Zn to preformed HIS, CPT: Coprecipitation of Zn during HIS synthesis.
[g] Final Zn/Al ratio in solid calculated from the total Zn content and assuming that all added Al was incorporated into HIS during synthesis.
[h] Zn coordinated to 6 second-neighbor Al (reference: Zn–HIS-1.6-pH6).
[i] Zn coordinated by 2 second-neighbor Al (reference: Zn-sorbed gibbsite-1.9).
[j] Outer-spherically sorbed Zn (reference: aqueous Zn).

was aged in a closed vessel for 14 days at 230 °C. Subsequently, the precipitate was washed 3 times and air-dried. The synthetic Zn-kaolinite had a Zn/Al ratio of 0.0006 (270 mg/kg Zn), indicating only limited Zn uptake into the kaolinite structure. Natural Zn-containing lithiophorite (“Zn-lithiophorite”, 180 mg/kg Zn) from Cornwall, Great Britain, was kindly provided by Beda Hofmann (Natural History Museum Bern, Switzerland). Lithiophorite (free of Zn) was synthesized according to (Feng et al., 1999). The structures of the kaolinites and lithiophorites were confirmed by XRD.

Gibbsite was synthesized as described in Kyle et al. (1975). Zn was adsorbed to gibbsite by reacting 1 g of gibbsite with 1 L of 0.1 M $NaNO_3$ containing 1 mM $Zn(NO_3)_2$ (24 h, pH 6.0). The Zn-sorbed gibbsite was filtered, washed, frozen in LN and freeze-dried. The final product contained 4000 mg/kg (“Zn-sorbed gibbsite-4.0”). An EXAFS spectrum of a similarly synthesized Zn-sorbed gibbsite containing 1900 mg/kg Zn (“Zn-sorbed gibbsite-1.9”) was kindly provided by Darryl Roberts (Roberts et al., 2003). Zn adsorbed to goethite was prepared by adding 800 mL solution of 1 mM $Zn(NO_3)_2{\cdot}4H_2O$ and 0.1 M $NaNO_3$ to 0.8 g of goethite (Schlegel et al., 1997). The suspension was titrated to pH 7.0 and reacted during 62 h, resulting in a Zn content of 2900 mg/kg. Preparation of Zn sorbed birnessite at low surface coverage (Zn/Mn = 0.003, “low Zn-birnessite”) has been described elsewhere (Jacquat et al., 2008).

## 2.4. EXAFS spectra acquisition

Bulk Zn K-edge EXAFS spectra were recorded at the XAS beamline at the Angströmquelle Karlsruhe (ANKA, Karlsruhe, Germany). The Si (111) monochromator was detuned by 35% using a software-controlled monochromator stabilization to reduce higher harmonics. The monochromator was calibrated by assigning the first maximum of the first derivative of the absorption edge of metallic Zn to 9659 eV. Powdered soil and reference samples were pressed into pellets with polyethylene or Licowax C®. They were analyzed at room temperature in fluorescence (5-element Ge solid state detector) or in transmission mode, depending on Zn concentration. Microspectroscopic analyses on a polished thin section of embedded aggregates of soil GRÜ were performed at the beamline 10.3.2 (Marcus et al., 2004) at the Advanced Light Source (ALS, Berkeley, USA). After the analysis of element distributions by μ-XRF spectrometry (see electronic annex for details), one Zn K-edge EXAFS spectrum was recorded using a beam size of $16 \times 7\ \mu m^2$.

## 2.5. EXAFS data extraction and analysis

Extraction of the EXAFS spectra from the raw data was performed using the software code Athena (Ravel and Newville, 2005). The $E_0$ was set to the maximum of the first derivative of the absorption edge. The spectra were normalized by subtracting a first order polynomial fit to the data before the edge (−150 to −30 eV relative to $E_0$) and subsequently dividing through a second order polynomial fit to the post-edge data (+150 eV up to 100 eV before end of spectrum). The EXAFS signal was extracted using a cubic spline function and the Autobk algorithm implemented in Athena ($R_{bkg} = 0.9$ Å, $k$-weight = 3, spline $k$-range from 0.5 to 12 $Å^{-1}$). The EXAFS spectra were Fourier-transformed over the $k$-range 2-10 $Å^{-1}$, using a Kaiser-Bessel apodization window (window parameter = 2.5).

Linear combination fits (LCF) were calculated following an approach and software developed by Manceau and coworkers (Manceau et al., 1996; Manceau et al., 2000; Marcus et al., 2004). Reference spectra for LCF were selected from an extensive database including crystalline Zn phases, Zn adsorbed to different mineral surfaces, and Zn complexed by organic molecules. Spectra were either recorded on own reference materials (Scheinost et al., 2002; Voegelin et al., 2005; Jacquat et al.,2008) or were provided by other researchers. In addition to the reference compounds described in Section 2.3, spectra considered for this study included Zn-layered double hydroxide (Zn-LDH), ZnMg-kerolite at various Zn/Mg ratios (Zn-kerolite, $Zn_{0.8}Mg_{0.2}$-kerolite, $Zn_{0.6}Mg_{0.4}$-kerolite, $Zn_{0.34}Mg_{0.66}$-kerolite, $Zn_{0.03}Mg_{0.97}$-kerolite), amorphous $Zn(OH)_2$, Zn adsorbed to goethite, Zn bearing birnessite with high (Zn/Mn ratio of 0.088) and low (Zn/Mn ratio of 0.003) coverage, Zn sorbed to ferrihydrite, Zn sorbed to calcite, Zn-phytate and aqueous Zn (0.5 M $ZnNO_3$, pH 6.0) (see electronic annex for details). The LCF analysis of the experimental spectra was carried out by calculating 1-component to 4-components fits. Starting from the best 1-component fit as judged by the lowest NSSR ($NSSR = (\Sigma_i(k^3\chi_{exp}\text{-}k^3\chi_{fit})^2)/\Sigma_i(k^3\chi_{exp})^2$), additional components were considered to substantially improve the fit as long as the NSSR decreased by at least 10% relative to the previous fit. The approximate precision of LCF with respect to the fractions of individual reference spectra has previously been estimated to 10% of the total Zn (Isaure et al., 2002). However, the detection limit, precision, and accuracy of LCF depend on the EXAFS amplitude of the species of interest, structural and spectral similarities between different species in mixtures, and the availability of a database including all relevant reference spectra (Manceau et al., 2000).

The EXAFS spectra of selected synthetic and natural reference materials were analyzed by shell fitting in *r*-space. Theoretical scattering paths were calculated with FEFF 8.40 (Ankudinov et al., 1998). Shell-fitting of Zn–HIS, Zn-sorbed gibbsite and aqueous Zn spectra was performed using Zn–O and Zn–Al paths calculated from the structure of gibbsite (Saalfeld and Wedde, 1974), by placing one Zn atom into a dioctahedral vacancy. For the analysis of Zn-kaolinite spectra, Zn–O, Zn–Al and Zn–Si single scattering paths were obtained by substituting one Al atom by Zn in the structure of kaolinite (Bish and Vondreele, 1989). Shell fits were calculated over the *r*-range 1–3 Å (or 1–2.1 Å for aqueous Zn) using the software code Artemis (Ravel and Newville, 2005). Path parameters were optimized by minimizing the normalized sum of squared residuals ($NSSR = (\Sigma_i(k^3\chi_{exp}\text{-}k^3\chi_{fit})^2)/\Sigma_i(k^3\chi_{exp})^2)$). The amplitude reduction factor $S_0$ was fixed to 0.85 (Teo, 1986) and the energy shift was constrained to be the same for all shells within individual fits.

### 2.6. Simulation of Zn K-edge EXAFS spectra for gibbsitic model clusters

Simulations of Zn K-edge EXAFS spectra were carried out for three different gibbsitic model clusters. Structural representations of the three clusters are provided in the electronic annex (Fig. EA4 to EA6). Using ATOMS (Ravel, 2001), the basic structure of all clusters was derived from the structure of talc (Perdikatsis and Burzlaff, 1981). After removing all Si atoms and replacing Mg by Al, three different gibbsitic clusters were constructed: (1) Gibbsitic cluster with one central Zn atom placed in the dioctahedral vacancy, all other vacancies unfilled (“unfilled gibbsitic cluster”). (2) Gibbsitic cluster with a central Zn atom placed in the dioctahedral vacancy, all other vacancies filled with Zn (“filled gibbsitic cluster”). (3) Gibbsitic cluster with one central Zn substituting for one Al atom (“substituted gibbsitic cluster”). Using FEFF 8.40 (Ankudinov et al., 1998), Zn K-edge EXAFS spectra were calculated for all thee gibbsitic clusters over different cluster sizes around the central Zn atom, limiting the maximum half-path distance to 8 Å and including either only single scattering (“SS”) or all single and multiple scattering paths with up to six legs (“SS+MS”). Based on shell-fits of experimental Zn–HIS spectra, the Debye-Waller parameter was fixed to 0.008 $Å^2$ for the first-shell single scattering Zn–O path and to 0.004 $Å^2$ for the second-shell Zn–Al and next nearest Zn–O (at ~3.28 Å) paths. For all other single- and multiple-scattering paths, the Debye Waller parameter was fixed to 0.008 $Å^2$. An energy shift of −7 eV was assigned to all paths (based on shell-fits of experimental Zn–HIS spectra).

### 2.7. Sequential extraction procedure

In order to assess the fractionation of Zn in the contaminated soils, the 7-step sequential extraction procedure (SEP) of Zeien and Brümmer (1989) was used. Experimental details are provided in Voegelin et al. (2008). Briefly, each soil was extracted in duplicates (2 g of soil each) according to the following sequence (with hypothetical interpretation according to Zeien and Brümmer (1989) in parentheses): Fraction F1: 1 M $NH_4NO_3$ (readily soluble and exchangeable); Fraction F2: 1 M $NH_4$-acetate, pH 6.0 (mobilizable and $CaCO_3$ bound); Fraction F3: 0.1 M $NH_2OH$-HCl + 1 M $NH_4$–acetate, pH 6.0 (Mn oxides); Fraction F4: 0.025 M $NH_4$-EDTA, pH 4.6 (bound to organic substances); Fraction F5: 0.2 M $NH_4$–oxalate, pH 3.25 (bound to amorphous and poorly crystalline Fe oxides); Fraction F6: 0.1 M ascorbic acid + 0.2 M $NH_4$–oxalate, pH 3.25 (bound to crystalline Fe oxides). All extraction steps were performed with a solution-to-soil ration of 25 mL/g. The solutions from the extraction steps F1 to F6 were analyzed by ICP-OES. The residual fraction F7 was determined by XRF spectrometry.

Different synthetic Zn-bearing phases (Zn–HIS-6.9-pH5, Zn-gibbsite-4.0, low Zn-birnessite and lithiophorite– see paragraph 2.3 for details on reference materials) were spiked into 2 g of quartz powder (Fluka®, Nr. 83340) to achieve contamination levels of 200, 250, 400 mg/kg Zn, and 3000 mg/kg Mn, respectively. The spiked quartz powders were homogenized for 24 h on an overhead shaker prior to sequential extraction.

### 2.8. Na-citrate extraction

In order to dissolve the hydroxy-Al interlayers of phyllosilicate minerals, the residual soil or quartz from the SEP (i.e. the residual material after step F6) was extracted

using the method of Tamura (1958). The same extraction was also performed with pure reference materials (Zn–HIS-6.9-pH5, Zn–HIS-2.1-pH5, and synthetic Zn-kaolinite, see paragraph 2.3 for details on reference materials) as well as with the <2 μm size fraction of the soils. The extractions were performed in duplicates using either 50 or 250 mg of material at a SSR of 200 ml/g. The samples were extracted for 1 h in boiling 0.3 M Na-citrate solution adjusted to pH 7.3. Subsequently, the extracts were separated by centrifugation (5 min, 3200 g), passed through nylon filters (0.45 μm) and acidified (1% v/v 30% $HNO_3$). After repeating this treatment two times, the three extracts were quantitatively merged and the Zn content analyzed by ICP-OES. The citrate-extracted soil clay fractions were Mg-saturated and analyzed by X-ray diffraction as described in Section 2.2.

## 3. RESULTS

### 3.1. Soil properties and mineralogy

Physical and chemical properties and Zn contents of the soil samples are provided in Table 1. The soils were contaminated with 251 to 1039 mg/kg Zn due to the input of aqueous Zn with the runoff water from power line towers that have been constructed 35 to 74 years ago. Upper levels of normal geogenic soil Zn contents in Switzerland are 57, 88, 95, 116, and 132 mg/kg for soils with pH ($CaCl_2$) of <4.3, 4.3-5.0, 5.1-6.1, 6.2-6.7, and 6.8-7.6, respectively (Keller and Desaules, 2001). The Zn contents of all soils except SAR and HAU exceeded these levels 7–12 fold, indicating substantial contamination from the power line towers. The Zn contents of the soils SAR and HAU exceeded the upper levels of normal geogenic soil Zn 2–3 fold, suggesting that these soils were also slightly contaminated with Zn.

XRD patterns of oriented mounts of the <2 μm size fraction of the soils GER, GRÜ and HAU are shown in Fig. 1. The mineralogy was dominated by hydroxy-interlayered minerals, kaolinite, illite and quartz. The 14.2 Å (6.2° 2θ Cu Kα) peak observed for all Mg-saturated slides did not collapse upon K-saturation and heating to 100 °C, but shifted to ~11.2 Å after heating to 550 °C, indicating that the interlayer space of the 14.2 Å mineral was filled with hydroxy-polymers (Barnhisel and Bertsch, 1989; Douglas, 1989). The 14 Å peak observed after heating the K-saturated clay fraction to 550 °C confirmed the presence of chlorite. Also after the removal of hydroxy-Al interlayers from soil clay minerals by Na-citrate extraction, ethylene glycol (EG) and glycerol (Gly) solvation did not cause a shift of the 14.2 Å peak to higher d-spacings (Fig. EA9), indicating that it originated mainly from hydroxy-interlayered vermiculite (HIV) rather than hydroxy-interlayered smectite (HIS). Accessory minerals observed included K-feldspar, plagioclase and goethite. Interstratified illite-vermiculite was also detected in the GER soil. XRD patterns collected on the clay fractions of the soils MOM, SAR, CHI, BUN and BIB2 are provided in the electronic annex (Figs. EA7 and EA8). The clay mineralogy of these soils were similar to the soils

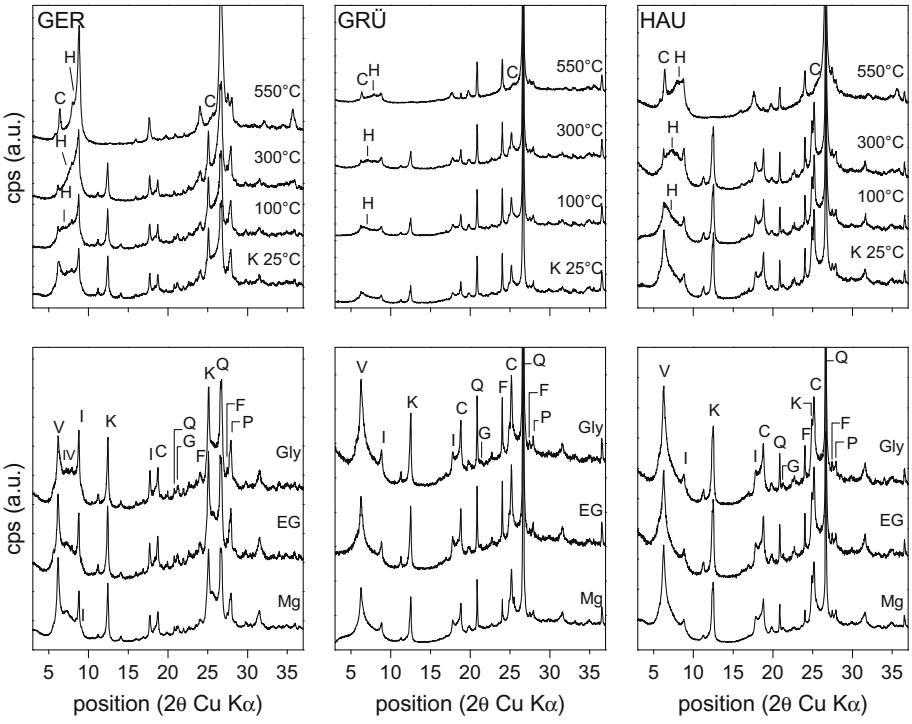


Fig. 1. X-ray diffraction patterns of oriented mounts of the <2 μm size soil fraction. Lower panels: Mg-saturated slides in air-dried state (Mg) and after ethylene glycol (EG) and glycerol solvation (Gly). Upper panels: K-saturated slides (K) after ex situ thermal treatment. C: chlorite; F: K-feldspars; G: goethite; H: hydroxy-interlayered vermiculite; I: illite; IV: interstratified mica-vermiculite; K: kaolinite; P: plagioclase; Q: quartz; V: vermiculite.

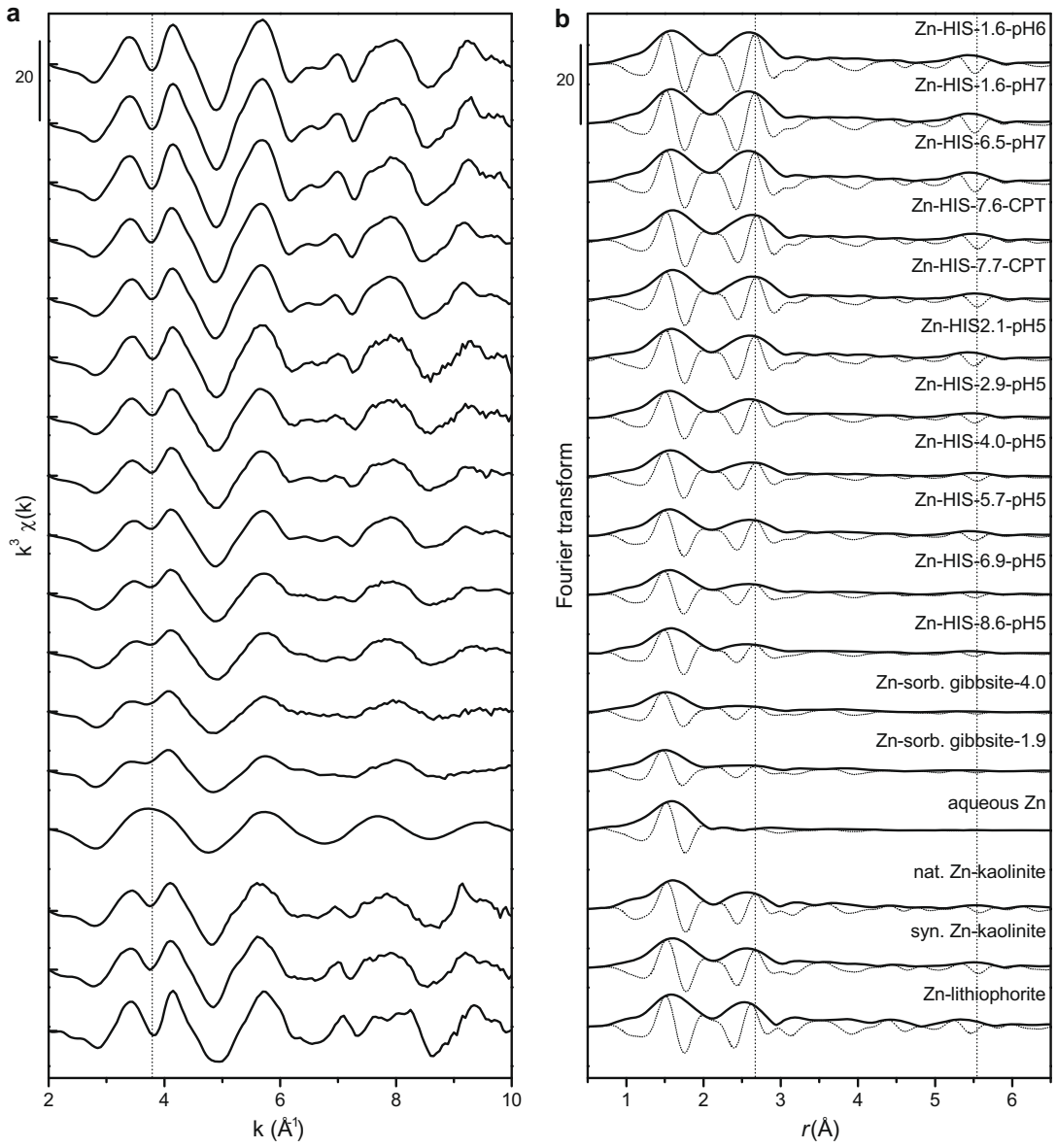


Fig. 2. EXAFS spectra (a) and Fourier transform magnitudes and imaginary parts (b) of synthetic Zn–HIS references, synthetic Zn-sorbed gibbsites, natural and synthetic Zn-kaolinites and natural Zn-lithiophorite. Vertical dashed lines are located at 3.79 Å$^{-1}$ (a) and 2.67 Å and 5.54 Å (b).

GER, GRÜ and HAU and were also characterized by a substantial fraction of HIV.

### 3.2. Uptake of Zn into HIS and local coordination from EXAFS spectroscopy

The Zn contents and final Zn/Al ratios of the synthetic Zn–HIS phases are listed in Table 2. Depending on synthesis pH, initial Zn/Al ratio, reaction time, and mode of Zn uptake, final Zn contents varied between 1615 and 8600 mg/kg (25 to 132 mmol/kg). These contents correspond to molar Zn/Al ratios of 0.013 to 0.087, indicating that only a minor fraction of total Zn had been incorporated at higher initial Zn/Al ratios. In addition to higher pH, factors that seemed to favored Zn incorporation were Zn coprecipitation rather than adsorption and increased equilibration time.

The EXAFS spectra and corresponding Fourier transforms of the Zn–HIS and Zn-sorbed gibbsite references are presented in Fig. 2. Results from shell fitting are provided in Table 3. A direct comparison of the spectra of Zn–HIS-1.6-pH6 and Zn-sorbed gibbsite-1.9 in *k*- and *r*-space is shown in Fig. 3. Zn–HIS samples synthesized at the lowest Zn/Al ratio and pH 6.0-7.0 (Zn–HIS-1.6-pH6, Zn–HIS-1.6-pH7, and Zn–HIS-6.5-pH7) as well as samples prepared by Zn coprecipitation (Zn–HIS-7.6-CPT and Zn–HIS-7.7-CPT) exhibited first-shell Zn–O distances of 2.06-2.08 Å and coordination numbers of 6.1-6.9. Second-shell

Table 3
Results from shell fits to the reference spectra shown in Fig. 2 (*r*-range 1 to 3 Å, fits are shown in Fig. EA2 and all fit parameters including their uncertainties are provided in Table EA1 in the electronic annex).

| Samples | Zn–O shell | | | Zn–Al shell | | | Zn–X shell | | | | $\Delta E_0$ (eV)[d] | NSSR (%)[e] |
|---|---|---|---|---|---|---|---|---|---|---|---|---|
| | $R_{Zn-O}$[a] | CN[b] | $\sigma^2$ (Å$^2$)[c] | $R_{Zn-Al}$[a] | CN[b] | $\sigma^2$ (Å$^2$)[c] | X | $R_{Zn-X}$[a] | CN[b] | $\sigma^2$ (Å$^2$)[c] | | |
| Zn–HIS-1.6-pH6 | 2.08 | 6.9 | 0.008 | 3.04 | 6.6[f] | 0.004[g] | O | 3.28 | 6.6[f] | 0.004[g] | 7.4 | 0.9 |
| Zn–HIS-1.6-pH7 | 2.08 | 6.8 | 0.007 | 3.04 | 6.6[f] | 0.004[g] | O | 3.28 | 6.6[f] | 0.004[g] | 7.1 | 1.0 |
| Zn- HIS-6.5-pH7 | 2.08 | 6.8 | 0.008 | 3.03 | 6.7[f] | 0.005[g] | O | 3.28 | 6.7[f] | 0.005[g] | 6.9 | 0.9 |
| Zn–HIS-7.6-CPT | 2.08 | 6.3 | 0.008 | 3.06 | 5.4[f] | 0.005[g] | O | 3.27 | 5.4[f] | 0.005[g] | 7.5 | 0.7 |
| Zn–HIS-7.7-CPT | 2.08 | 6.1 | 0.008 | 3.06 | 4.7[f] | 0.004[g] | O | 3.28 | 4.7[f] | 0.004[g] | 7.9 | 0.8 |
| Zn–HIS-2.1-pH5 | 2.08 | 6.1 | 0.008 | 3.04 | 4.6[f] | 0.004[g] | O | 3.27 | 4.6[f] | 0.004[g] | 7.4 | 0.8 |
| Zn–HIS-2.9-pH5 | 2.07 | 6.3 | 0.010 | 3.04 | 3.9[f] | 0.004[g] | O | 3.28 | 3.9[f] | 0.004[g] | 6.9 | 0.9 |
| Zn–HIS-4.0-pH5 | 2.07 | 6.1 | 0.010 | 3.04 | 3.6[f] | 0.005[g] | O | 3.28 | 3.6[f] | 0.005[g] | 6.9 | 0.8 |
| Zn–HIS-5.7-pH5 | 2.07 | 5.8 | 0.009 | 3.05 | 3.1[f] | 0.004[g] | O | 3.27 | 3.1[f] | 0.004[g] | 7.2 | 0.7 |
| Zn–HIS-6.9-pH5 | 2.06 | 5.8 | 0.010 | 3.04 | 2.6[f] | 0.005[g] | O | 3.29 | 2.6[f] | 0.005[g] | 6.9 | 0.8 |
| Zn–HIS-8.6-pH5 | 2.06 | 5.3 | 0.008 | 3.04 | 2.1[f] | 0.004[g] | O | 3.30 | 2.1[f] | 0.004[g] | 8.0 | 1.0 |
| Zn-sorb. gibbsite-4.0 | 2.04 | 5.8 | 0.013 | 3.01 | 1.7[f] | 0.005[g] | O | 3.28 | 1.7[f] | 0.005[g] | 4.6 | 0.9 |
| Zn-sorb. gibbsite-1.9 | 2.03 | 5.8 | 0.012 | 3.01 | 1.7[f] | 0.005[g] | O | 3.26 | 1.7[f] | 0.005[g] | 3.6 | 0.9 |
| Aqueous Zn | 2.08 | 6.3 | 0.008 | — | — | — | — | — | — | — | 6.1 | 0.2 |
| nat. Zn-kaolinite | 2.09 | 5.9 | 0.008 | 3.05 | 4.3 | 0.004[g] | Si | 3.16 | 1.4[h] | 0.004[g] | 7.1 | 1.1 |
| syn. Zn-kaolinite | 2.10 | 6.5 | 0.008 | 3.05 | 6.9 | 0.009[g] | Si | 3.13 | 2.3[h] | 0.009[g] | 7.2 | 1.1 |
| Zn-lithiophorite | 2.07 | 6.3 | 0.007 | 2.99 | 4.5[f] | 0.002 | O | 3.27 | 4.5[f] | 0.004 | 7.3 | 0.7 |

[a] Radial distance; uncertainties are ~0.01 Å for Zn–O, 0.01–0.03 Å for Zn–Al, and 0.04–0.08 Å for Zn–X shells, except Zn–X in Zn-kaolinite samples with uncertainty of 0.2 Å.
[b] Coordination numbers; uncertainties are 0.5–1.5 for Zn–O and 0.7–2.4 for Zn–Al/X shells.
[c] Debye Waller parameters; uncertainties are ~ 0.002 Å$^2$ for Zn–O.
[d] Energy shift; set equal for all shells in a fit, uncertainties are 0.1–2.5 eV.
[e] Normalized sum of the squared residuals (NSSR = $\Sigma(data_i–fit_i)^2/\Sigma(data_i)^2$).
[f,g] Set equal for Zn–Al and Zn–X path within individual fit.
[h] CN of Si constrained to 1/3 of CN of Al during fit.

Zn–Al distances varied between 3.03-3.06 Å and coordination numbers between 4.7 and 6.6. These data suggest that octahedrally coordinated Zn was predominantly incorporated in the dioctahedral vacancies of gibbsitic hydroxy-Al polymers, i.e., as a hexadentate complex surrounded by 6 second-neighbor Al atoms (see Figs. EA4 and EA5 in the electronic annex). In the spectra, this was phenomenologically reflected in the splitting of the first EXAFS oscillation at 3.8 Å$^{-1}$ and in the coincidence of the maxima of the Fourier transform magnitude and imaginary part of the second shell (Scheinost et al., 2002; Manceau et al., 2004; Schlegel and Manceau, 2007).

Shell fits to the spectra of Zn adsorbed to gibbsite returned a second-shell Zn–Al distance of 3.01 Å and a coordination number of 1.7. In *r*-space, the magnitude of the first shell of the spectrum of Zn-sorbed gibbsite-1.9 was clearly lower than for Zn–HIS-1.6-pH6 and the imaginary part was shifted to slightly lower r (Fig. 3). In the fits, these differences were reflected in a lower first-shell Zn–O distance (2.03 versus 2.08 Å), a lower coordination number (5.8 versus 6.9), and a higher Debye-Waller parameter (0.012 versus 0.008 Å$^2$) for Zn-sorbed gibbsite-1.9 than Zn–HIS-1.6-pH6 (Table 3). In agreement with previous studies (Roberts et al., 2003; Schlegel and Manceau, 2007), these fitting results suggest that Zn sorbed to gibbsite was mainly octahedrally and to a lesser extent tetrahedrally coordinated with O, forming mainly mononuclear bidentate (i.e., edge-sharing) sorption complexes with Al octahedra at the surface of gibbsite. Aqueous Zn is shown in Fig. 2 as a proxy for Zn sorbed as an outer-sphere complex. The Zn–O coordination number and distance obtained from shell fitting confirm the octahedral coordination of hydrated $Zn^{2+}$.

The EXAFS spectra of Zn–HIS phases synthesized at pH 5.0 by adsorption of Zn to preformed HIS show a gradual transition from the first group of spectra (octahedral Zn in the vacancy of gibbsitic hydroxy-Al polymers) to Zn-sorbed gibbsite (mainly octahedrally coordinated Zn forming bidentate edge-sharing sorption complexes) and/or aqueous Zn (exchangeable Zn) (Fig. 2). This trend was reflected by shell fits indicating a gradual decrease in second-shell Zn–Al coordination number with increasing Zn-loading of the HIS (Tables 2 and 3). LCF analysis confirmed that all Zn–HIS spectra could be well reproduced by one- to three component fits using the spectra Zn–HIS-1.6-pH6, Zn-sorbed gibbsite-1.9, and aqueous Zn (Table 2, LCF shown in Fig. EA2 in the electronic annex). The fractions of Zn–HIS-6.9-pH5 returned by LCF varied systematically with Zn–HIS composition and were nearly independent on whether only Zn-sorbed gibbsite-1.9, only aqueous Zn, or both spectra were present in the fit. On the other hand, the relative fractions of Zn-sorbed gibbsite-1.9 and aqueous Zn varied considerably (Table 2), which may have been due to the spectral similarity of these references. Nevertheless, both Zn-sorbed gibbsite-1.9 and aqueous Zn were needed for good LCF, especially for the spectra of Zn–HIS prepared by adsorption of Zn at pH 5.0. Overall, the LCF results indicated

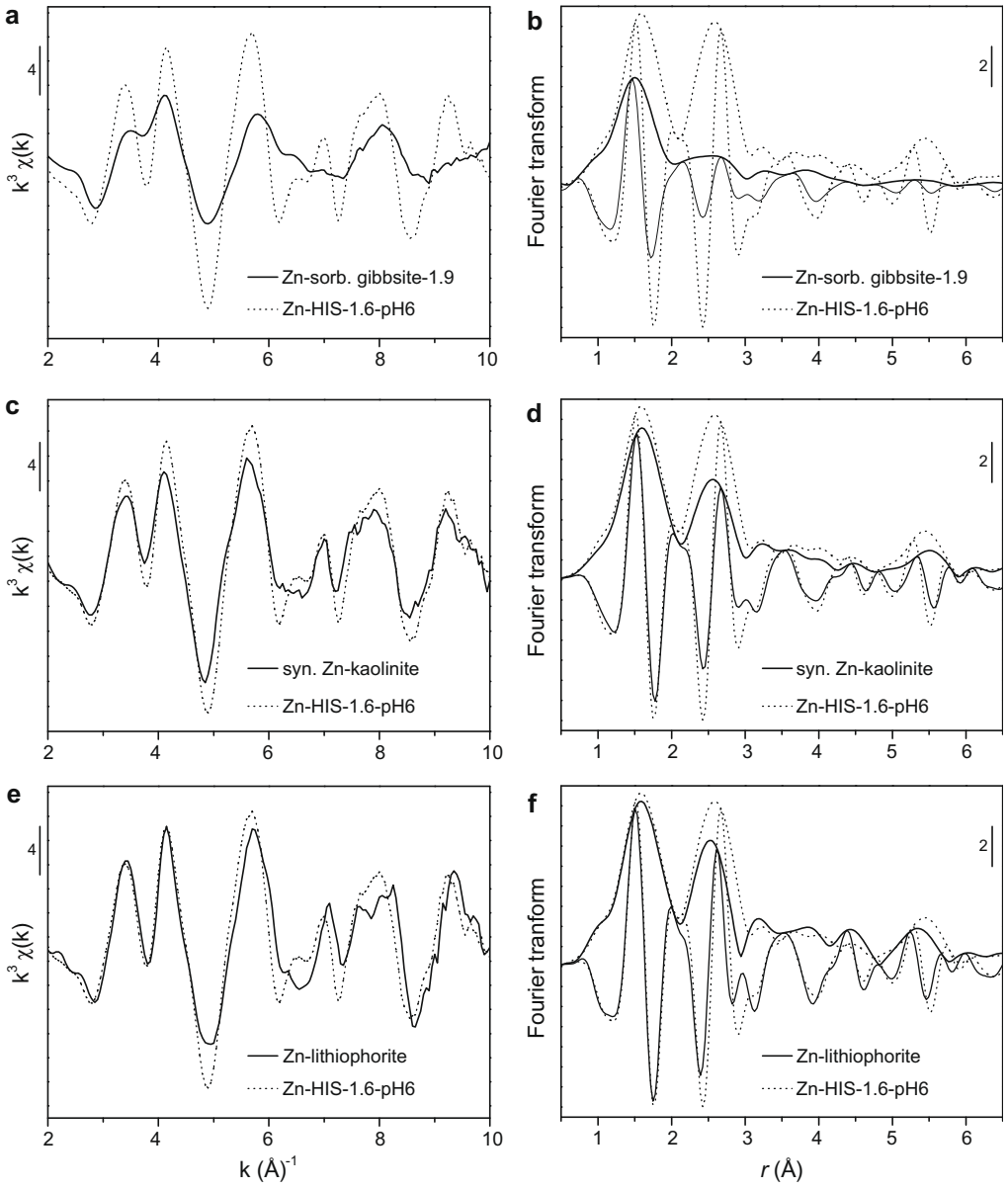


Fig. 3. Comparison of the EXAFS spectra of Zn–HIS-1.6-pH6.0 with: Zn-sorbed gibbsite-1.9 (a, b), synthetic Zn-kaolinite (b, d) and Zn-lithophorite (e, f) in *k*-space and in *r*-space, respectively.

that the dominant factor favoring the sorption of Zn in the vacancies of hydroxy-Al polymers was the molar ratio Zn/Al during synthesis. Under otherwise identical conditions, increasing Zn loading of HIS resulted in the sorption of Zn to Al-polymer sites with decreasing Al coordination as well as to cation exchange sites. In addition to low Zn/Al ratios in the Zn–HIS, other factors that favored Zn incorporation into hydroxy-Al vacancies included higher pH and coprecipitation of Zn during HIS synthesis instead of Zn adsorption to preformed HIS (Table 2). The Zn–HIS samples synthesized by Zn adsorption at pH 5.0 were washed with DI water prior to drying, which may have removed some exchangeable Zn. Thus, the measured Zn contents and the fractions of exchangeable Zn estimated from LCF fits may be somewhat lower than during contact of the HIS with the Zn-containing solution.

### 3.3. EXAFS simulations for gibbsitic model clusters: Effect of Zn location and loading

In order to extend our preceding EXAFS interpretation by shell-fitting and to assess the effect of Zn incorporation in various positions within gibbsitic structures on the EXAFS signal, we performed a series of EXAFS simulations for gibbsitic model clusters (structures depicted in Figs. EA4-EA6, electronic annex). Simulation results in *k*- and *r*-space are presented in Fig. 4. First, we considered a gibbsitic cluster containing one Zn atom located in a dioctahedral vacancy, with all other vacancies unfilled

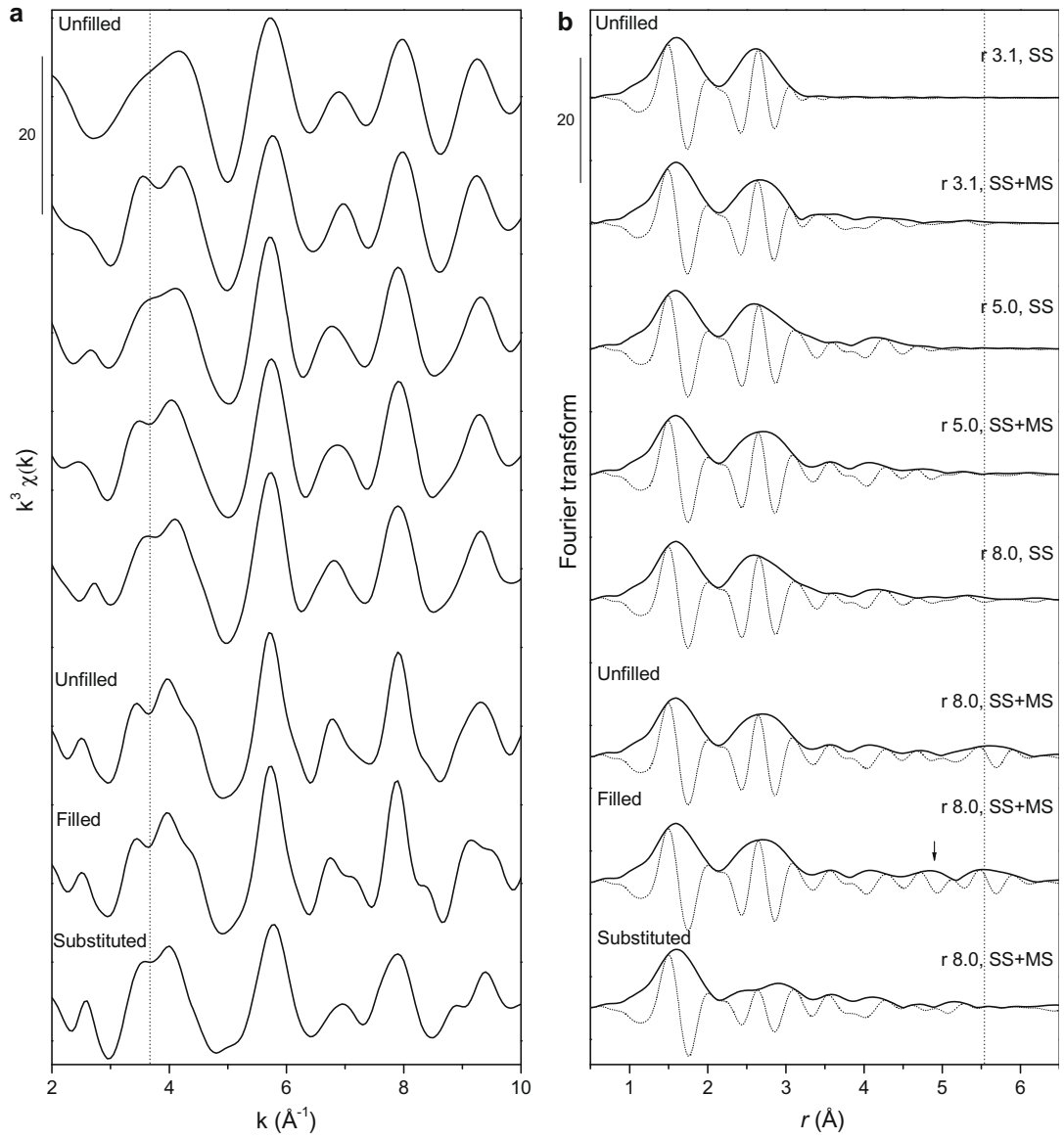


Fig. 4. Simulated EXAFS spectra for Zn in gibbsitic model clusters. Simulations were carried out over increasing cluster sizes (r in Å) including only single scattering (SS) or single and multiple scattering (SS+MS). *Unfilled*: Zn atom in octahedral vacancy of gibbsitic Al-cluster. *Filled*: All dioctahedral vacancies filled with Zn (arrow indicates 4.9 Å peak from Zn-Zn scattering contributions). *Substituted*: Zn substituting for Al in gibbsite structure. The cluster structures are shown in Figs. EA4-EA6 in the electronic annex. Vertical dashed lines are located at 3.67 Å$^{-1}$ (a) and 5.54 Å (b).

("Unfilled"). Calculations for increasing cluster sizes up to 8 Å based on single scattering ("SS") or including multiple scattering ("SS+MS") (with maximum half path lengths of 8 Å) did not properly reproduce the splitting of the first EXAFS oscillation at 3.8 Å$^{-1}$ (Fig. 2a). The comparison of the Fourier-transformed EXAFS spectrum of Zn–HIS-1.6-pH6 backtransformed over increasing *r*-ranges (Fig. EA3, electronic annex) indicated that this splitting mainly originated from scattering in the *r*-range 3.1-5.0 Å (not phase-shifted), which includes single-scattering from O atoms as well as multiple-scattering paths involving O and Al. Correct simulation of this splitting would thus require the 3-dimensional refinement of the gibbsitic structure around the central Zn atom, which was beyond the scope of this study. However, the simulations over a cluster size of 8 Å without and with multiple scattering clearly indicated that the peak at 5.5 Å in the Fourier transform resulted mainly from focused multiple scattering along the 6 collinear Zn–Al-Al axes (Fig. EA4), as typically observed in octahedral sheets (O'Day et al., 1994; Juillot et al., 2006; Schlegel and Manceau, 2006).

A simulation over a radius of 8.0 Å including single and multiple scattering was also performed with a gibbsitic cluster whose dioctahedral vacancies were all filled with Zn ("Filled", Fig. 4). Compared to the unfilled gibbsitic cluster, the presence of 6 Zn atoms at a distance of 5.3 Å from the central Zn atom resulted in an additional peak in the Fourier transform at 4.9 Å (Fig. 4). This peak is not

observed in the experimental spectra of Zn–HIS (Fig. 2), suggesting that Zn atoms do not occupy adjacent vacancies in gibbsitic hydroxy-Al polymers of HIS. This compares with the low final Zn/Al ratio of all Zn–HIS references (Table 2), indicating that individual Zn atoms in the hydroxy-Al polymers were separated from each other. The lack of detectable next-nearest cationic Zn-Zn pairing in hydroxy-Al polymers may be due to charge repulsion, due to the structural distortion invoked by filling octahedral vacancies with Zn, or due to the limited size of the gibbsitic clusters in HIM.

The last simulation was performed for a gibbsitic cluster in which Zn substitutes for an Al atom ("Substituted", Fig. 4). In this cluster, Zn is surrounded by 3 Al atoms at 3.05 Å, 6 Al atoms at 5.3 Å and 3 Al atoms at 6.1 Å. Compared to the gibbsitic clusters with Zn incorporated into the dioctahedral vacancy, the substituted cluster has a lower number of Al atoms coordinated at a distance of 6.1 Å and does not exhibit any collinear Zn–Al–Al arrangement. Therefore, no peak is observed in the Fourier transform at 5.5 Å. Considering Zn–HIS synthesized at near neutral pH and low initial Zn/Al ratio, the presence of a pronounced peak at 5.5 Å in the Fourier transformed spectra (Fig. 2) in combination with the high second shell Zn–Al coordination numbers obtained from shell fits (Table 3) thus unequivocally show that Zn has been taken up into the vacancies of the gibbsitic structures.

### 3.4. Local coordination of Zn in Zn-kaolinite and Zn-lithiophorite

The EXAFS spectra of Zn-kaolinite and Zn-lithiophorite resemble the spectra of Zn–HIS (Fig. 2), reflecting the similarity in the local coordination of Zn. First-shell Zn–O distances (2.09-2.10 Å) and coordination numbers (5.9-6.5) obtained for Zn-kaolinite indicate that Zn was octahedrally coordinated (Table 3). Compared to the Zn–HIS reference, the EXAFS oscillations of synthetic (and natural) Zn-containing kaolinite were shifted to slightly lower *k*-values and the left side of the second oscillation in *k*-space showed a curvature at 5.2 $Å^{-1}$ which was absent in the Zn–HIS-1.6-pH6 reference spectrum (Fig. 3c). Compared to the Zn–HIS-1.6-pH6 spectrum, synthetic Zn-kaolinite exhibited a much lower second shell amplitude (Fig. 3d). This could partly be due to destructive interference with backscattering contributions from Si (Manceau and Calas, 1986; Manceau et al., 2005; Juillot et al., 2006). However, also the peak at 5.5 Å resulting from single and multiple focused scattering along collinear Zn–Al–Al arrangements is much lower (Fig. 3). Considering the simulations of EXAFS spectra of gibbsitic model clusters (Fig. 4), these differences suggest that Zn uptake into kaolinite may have partly been due to incorporation into vacant dioctahedral sites and partly due to substitution for Al.

The EXAFS oscillations of Zn-lithiophorite show a shift to higher *k*-values with respect to the ones of Zn–HIS-1.6-pH6 (Fig. 3e). In *r*-space, the imaginary part of the second shell of lithiophorite was shifted to lower r (Fig. 3f), consistent with a shorter Zn–Al distance (2.99 versus 3.04 Å, Table 3), as reported in previous work (Manceau et al., 2005).

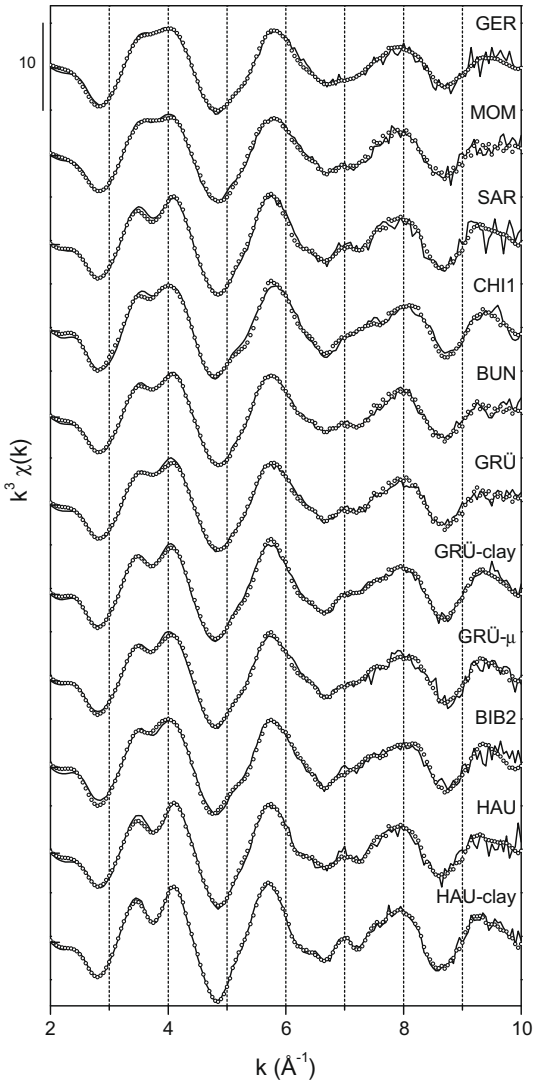


Fig. 5. EXAFS spectra of bulk soils, soil clay fractions and the clayey matrix in a thin section of soil GRÜ (solid lines) and LCF spectra (open dots). LCF results are provided in Table 4.

### 3.5. Analysis of the soil EXAFS spectra by LCF

The EXAFS spectra of all soil samples, the clay fractions of soils GRÜ and HAU, and a µ-EXAFS spectrum from soil GRÜ are shown in Fig. 5. For the soil GRÜ, nearly identical spectra were observed for the bulk soil, the clay fraction (GRÜ-clay) and the clayey matrix in a soil thin section (GRÜ-µ), in which Zn was evenly distributed within the clayey soil matrix (Fig. EA10). Also for soil HAU, nearly identical spectra were obtained from the bulk soil and the clay size fraction.

The first EXAFS oscillation of all spectra is split at 3.8 $Å^{-1}$, similarly as in the Zn–HIS, Zn-sorbed gibbsite, Zn-kaolinite and Zn-lithiophorite reference spectra (Figs. 2 and 5). Consequently, we selected these reference spectra for the analysis of the soil spectra by LCF. Adsorbed/complexed Zn-species and Zn-bearing precipitates such as Zn-LDH or ZnMg-kerolite phases with 3% to 100%

Table 4
Linear combination fits of EXAFS spectra from soils, soil clay fractions, and a thin section of soil GRÜ (shown in Fig. 5).

| Spectrum | Zn–HIS-6.9-pH5 (%) | Zn-kerolite[a] (%) | Sorbed $^{VI}$Zn[c] (%) | Sorbed $^{IV}$Zn[d] (%) | Sum (%) | NSSR (%) |
|---|---|---|---|---|---|---|
| GER | 29 | 18 (80Zn) | 31 (Aq) | 29 (Ph) | 107 | 3.87 |
| MOM | 36 | — | 22 (Aq) + 43 (Go) | — | 101 | 3.78 |
| SAR | 75 | 24 (60Zn) | — | — | 99 | 5.05 |
| CHI | 34 | 48 (60Zn) | — | 16 (Ph) + 16 (Bi) | 114 | 2.32 |
| BUN | 54 | 15 (34Zn) | 33 (Go) | — | 102 | 2.16 |
| GRÜ | 52 | 13 (60Zn) | 36 (Go) | — | 101 | 2.50 |
| GRÜ-clay | 61 | 39 (60Zn) | — | — | 100 | 2.08 |
| GRÜ-μ | 48 | 38 (60Zn) | — | 16 (Bi) | 102 | 3.52 |
| BIB2 | 50 | 24 (60Zn) | 29 (Go) | — | 103 | 3.56 |
| HAU | 84 | 15 (60Zn) | — | — | 99 | 4.50 |
| HAU-clay | 53 | 21 (60Zn) + 29 (Ka) | — | — | 103 | 1.37 |

[a] (80Zn), $Zn_{0.8}Mg_{0.2}$-kerolite, (60Zn), $Zn_{0.6}Mg_{0.4}$-kerolite, (34Zn), $Zn_{0.34}Mg_{0.66}$-kerolite, (Ka) synthetic Zn-kaolinite.
[c] (Aq), Aqueous Zn, (Go), Zn-sorbed goethite.
[d] (Ph), Zn-phytate, (Bi), low Zn-birnessite (Zn/Mn = 0.003).

Zn/(Zn+Mg) content were also included in the LCF analysis. In the EXAFS spectra of adsorbed/complexed Zn-species, the first shell Zn–O contribution may dominate the overall shape of the EXAFS signal due to weak backscattering contributions from second shell neighbors caused by low coordination numbers, disorder, or cancellation effects. As a result, clear distinction between different adsorbed/complexed species is complicated in soil spectra with several contributions. In LCF, we therefore only referred to octahedrally coordinated sorbed Zn (“sorbed $^{VI}$Zn”) and tetrahedrally coordinated sorbed Zn (“sorbed $^{IV}$Zn”) using the reference providing the lowest NSSR. While sorbed $^{VI}$Zn may either be specifically or electrostatically bound, sorbed $^{IV}$Zn only occurs as inner-sphere complex. For LCF, we used Zn sorbed goethite (octahedrally coordinated Zn forming inner-sphere sorption complex (Schlegel et al., 1997)) and aqueous Zn as proxies for sorbed $^{VI}$Zn. For sorbed $^{IV}$Zn, we used reference spectra of Zn-phytate (proxy for Zn bound to organic phosphate groups (Sarret et al., 2002)) and Zn sorbed birnessite at low surface coverage. In addition, Zn sorbed calcite (tetrahedral Zn, (Elzinga and Reeder, 2002)) was included in LCF of soils with pH > 5, but never occurred in the best LCF.

Overall, LCF indicated that Zn–HIM, Zn-containing phyllosilicates (ZnMg-kerolite phases) and adsorbed Zn are the major Zn species in the studied soils (Fig. 5. and Table 4). No Zn-LDH was detected by LCF in any of the studied soils. Since only HIV but no HIS was detected in the studied soils, we assume the fitted Zn–HIS fractions to correspond to Zn-HIV. While all Zn–HIS references depicted in Fig. 2 were used for LCF, best fits were consistently achieved with the reference Zn–HIS-6.9-pH5. This suggests that uptake of Zn into HIM tends to result in relatively similar local Zn coordination in HIM in all soils. For most soils, LCF results also indicated the presence of Zn in phyllosilicates with intermediate to high Zn/Mg ratio (represented by ZnMg-kerolite as structural proxies). However, except for soil CHI1, the fractions of Zn–HIM always exceeded the ZnMg-kerolite fraction. While LCF returned no sorbed Zn for the soils HAU and SAR with lowest Zn contents, the highest fractions of sorbed Zn were found for the two most acidic soils GER (60%) and MOM (65%). LCF returned similar results for the soils BUN, GRÜ and BIB2, likely reflecting their comparable soil physicochemical properties and Zn contents (Table 1). For the clay fraction of soil HAU, the best two-component fit was achieved with Zn–HIS-4.0-pH5 and $Zn_{0.6}Mg_{0.4}$-kerolite (71% and 31%, respectively, NSSR 2.34%). Adding synthetic Zn-kaolinite as a third reference reduced NSSR by more than 40% and visually improved the fit in the region of Zn–Si backscattering (3 to 4.5 Å in *r*-space, data not shown). For the validation of this result, however, direct identification of Zn-kaolinite within the soil matrix would be needed, e.g., using spatially resolved μ-EXAFS spectroscopy.

### 3.6. Sequential and Na-citrate extractions

Sequential extraction results are presented in Fig. 6. The percentage of exchangeable Zn (fraction F1) systematically decreased with increasing soil pH, from > 30% in the acidic soils GER and MOM to <1% in the soils BIB2 and HAU with pH > 6. Regardless of soil pH, between 49 to 66% of the total Zn was found in the last two fractions (F6+F7), indicating that most Zn was present in stable form. The additional Na-citrate extraction step mobilized large fractions (40-80%) of the residual Zn after the extraction step F6.

From Zn–HIS-6.9-pH5 spiked into quartz powder, about 30% of the Zn was extracted in the first extraction step, showing that this reference contained also exchangeable Zn. The remainder of the Zn was fractionated into F5 – F7. The stepwise dissolution of Zn–HIS using oxalate solutions is consistent with the study of Farmer et al. (1988) showing that the release of oxalate-soluble Al in podzolic soils is related to the extraction of pedogenic hydroxy-Al interlayers of HIV. Na-citrate treatment almost completely removed the Zn remaining after F6. Similarly, extraction of pure Zn–HIS-6.9-pH5 and Zn–HIS-2.1-pH5 with Na-citrate released > 78% of the total Zn (results not shown). In contrast, Na-citrate treatment only released 15% of the total Zn from synthetic Zn-kaolinite, confirming the high

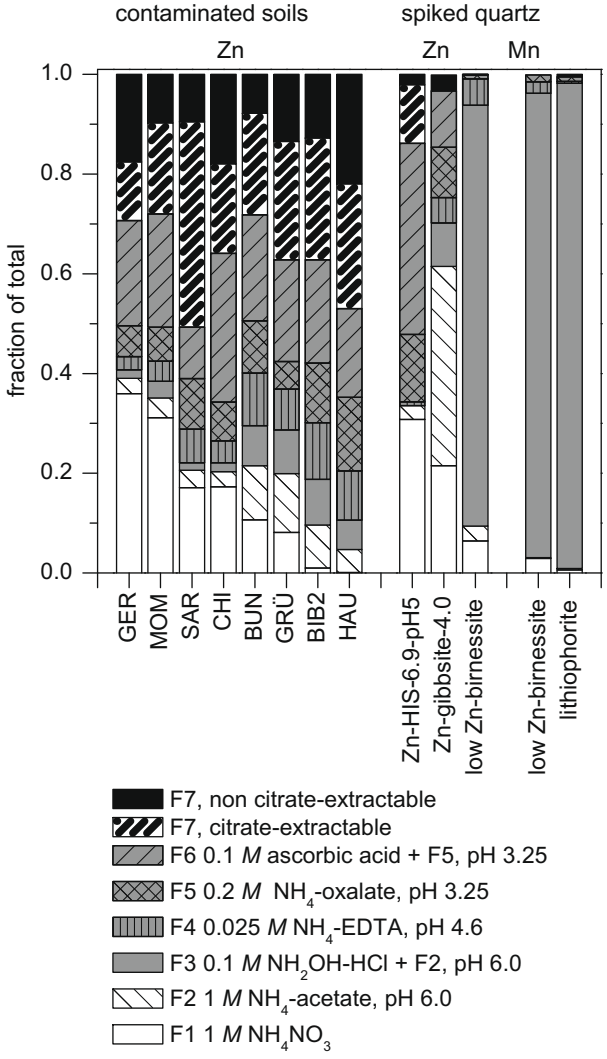


Fig. 6. Sequential extraction of contaminated soil materials and of quartz powder spiked with Zn–HIS-6.9-pH5, Zn-gibbsite-4.0, low Zn-birnessite and lithiophorite. Note: The citrate extraction was only performed on the residual of the sequentially extracted soils (after F6) and on Zn–HIS-6.9-pH5 spiked quartz. For references spiked into quartz, fractionation results are presented for Zn and/or Mn.

selectivity of citrate for hydroxy-Al polymers. From Zn-sorbed gibbsite spiked into quartz powder, about 60% of the total Zn were extracted in the first two steps of the SEP. In comparison with the data for Zn–HIS-6.9-pH5, this indicates that Zn sorbed to hydroxy-Al polymers in clays is more strongly retained than Zn sorbed to gibbsite, in agreement with previous work (Keizer and Bruggenwert, 1991). The SEP results thus suggest that Zn sorption to aluminium (hydr)oxides was not dominant in the studied soils. The hydroxylamine hydrochloride ($NH_2OH$-HCl) solution used in F3 selectively dissolved birnessite and lithiophorite, as previously reported (Chao, 1972). In the soils, little Zn was extracted in F3 (2-9% of total Zn), suggesting that only a minor fraction of Zn was sorbed to or incorporated into Mn-bearing minerals.

## 4. DISCUSSION

### 4.1. Sorption of Zn in hydroxy-interlayered minerals

The sorption of Zn to HIS as a function of hydroxy-Al loading, solution pH, and Zn concentration has previously been studied by Janssen and coworkers (Janssen et al., 2003a; Janssen et al., 2003 b). They found that the formation of hydroxy-Al interlayers reduces the cation exchange capacity, but provides high-affinity sorption sites for Zn. Thus, sorption of Zn to HIS could be modeled as a combination of high-affinity sorption of Zn to Al-polymers and cation exchange to the interlayer-free portions of the HIS. The extent of specific Zn sorption increased with Al-loading and solution pH. These results were obtained from experiments with Wyoming Clay Spur montmorillonite. The same type of clay material was also used by Schlegel and Manceau (2007). It has a $N_2$-BET surface are of $\sim$31 $m^2/g$ similar to the Wyoming montmorillonite SWy-2 (van Olphen and Fripiat, 1979; Bradbury and Baeyens, 1998), which has been used in the current study and the work by Scheinost et al. (2002). Thus, the results from Zn uptake studies by Janssen et al. (2003a) can be compared to the local coordination of Zn derived from EXAFS data obtained with a similar clay mineral.

The analysis of the EXAFS spectra (Fig. 2, Table 3) demonstrated that the local coordination of Zn sorbed to Al-polymers depends on solution pH, initial Zn/Al ratio, mode of Zn uptake, and reaction time. In general, higher pH, lower initial Zn/Al ratio, and Zn coprecipitation instead of adsorption seems to favor the bonding of Zn as a hexadentate complex in the vacancies of gibbsitic Al-polymers. As the Zn loading of the Zn–HIS phases increased with high Zn/Al ratio or longer incubation time, uptake shifted to sorption at sites with decreasing Al coordination and to uptake by cation exchange (Table 2). Differentiation between these two trends by LCF was complicated, because they both had similar effects on the shape of the EXAFS spectra (reduced second shell and higher shell signals compared to Zn incorporated into dioctahedral vacancies). According to Janssen et al. (2003b), uptake of Zn by cation exchange only becomes relevant once sorption to Al-polymers approaches its maximum.

At a hydroxy-Al loading of 2 mol/kg, i.e., the same as for to the HIS phases studied in this work, sorption at pH 5.0 was reported to reach a maximum of 80 mmol/kg specifically sorbed and 80 mmol/kg exchangeable Zn (Janssen et al., 2003 b). At pH 6.6, maximum uptake reached 250 mmol/kg specifically sorbed and 130 mmol/kg exchangeable Zn (Janssen et al., 2003 b). Thus, the Zn–HIS samples synthesized at pH 6.0 and 7.0 at low Zn/Al ratio were loaded with Zn at levels far below the maximum for high-affinity uptake, as reflected in the high coordination numbers. In Zn–HIS synthesized by adsorption of Zn to HIS at pH 5.0, however, the samples with highest loadings exceeded the maximum for specific sorption (80 mmol/kg, 5200 mg/kg) indicated by Janssen et al. (2003 b). Based on this limit for specific Zn uptake, 23% of the Zn in the sample Zn–HIS-6.9-pH5 would be expected to be exchangeably adsorbed. This compares to a fitted

fraction of outer-sphere aqueous Zn of 16% (Table 2) and an exchangeable (F1) fraction of ~30% released by sequential extraction (Fig. 6). However, some exchangeable Zn may have been lost from these samples (Zn–HIS with Zn adsorbed at pH 5.0 at high initial Zn/Al ratios) as they were washed with DI water after reaction with Zn-containing solution, possibly causing a reduction in the sorbed amount of Zn and the fraction of exchangeable Zn relative to the HIS in contact with the Zn-containing solution.

The shift in Zn speciation with Zn-loading reflects that hydroxy-Al polymers form island-like structures rather than complete gibbsitic interlayer sheets (Barnhisel and Bertsch, 1989; Meunier, 2007), in which Zn could only be incorporated into the dioctahedral vacancies. Complete hydroxy-Al interlayers cannot form in HIM because, as the degree of Al-polymerization increases, the positive charge of the interlayer becomes negligible and the negative charge of the 2:1 layers cannot be balanced (Meunier, 2007). Based on the stoichiometry of the montmorillonite SWy-2 ($[Al_{3.02}Fe_{0.41}Mn_{0.01}Mg_{0.54}Ti_{0.02}][Si_{7.98}Al_{0.02}]O_{20}(OH)_4$) and assuming a maximum of 4 Al atoms in the hydroxy-interlayer per unit cell, the filling of the interlayers of the synthetic HIS with hydroxy-Al (2 mmol/g montmorillonite) reached 37% of a complete gibbsite sheet. An average filling of 78% has been reported from the analysis of HIM contained in 12 Alabama soils (Kirkland and Hajek, 1972). These hydroxy-Al polymers may be arranged as polymer chains and partial cyclic polymers (Meunier, 2007), offering a variety of sorption sites for Zn with different degree of Al coordination. The EXAFS results suggest that Zn occupies these sites in the order of decreasing Al coordination. Interestingly, the coprecipitation of Zn with hydroxy-Al led to a higher final Zn/Al ratio and higher Zn–Al coordination than sorption of Zn to preformed HIS under otherwise comparable conditions (Zn–HIS-7.7-CPT versus Zn–HIS-5.7-pH5, Tables 2 and 3). This could indicate that the incorporation of $Zn^{2+}$ into the gibbsitic polymers during HIS formation partly compensated the loss of positive charge due to Al polymerisation, enhancing the formation of cyclic Zn-containing hydroxy-Al polymers.

### 4.2. Retention of Zn in hydroxy-interlayered phyllosilicates in soils

Analysis of the soil EXAFS spectra by LCF indicated that Zn in all soils was to a substantial extent sequestered into Zn–HIM (Table 4, proxy Zn–HIS-6.9-pH5). Since only HIV, but no HIS was detected in the studied soils, we assume Zn–HIM in these soils to mainly correspond to Zn-HIV. The highest percentages of Zn–HIM (75-84%) were detected in the soils HAU and SAR which had the lowest Zn contents (Table 1). In the soils BUN, GRÜ and BIB, which all had an intermediate soil pH and similar organic C, clay and Zn contents, about half (50-54%) of the total Zn was present as Zn–HIM. The lowest fractions of Zn–HIM (29-34%) were found in the soils GER, MOM, and CHI1 with low pH and clay contents. The percentages of Zn sorbed to other soil components than HIM decreased from the soils GER and MOM (60-65%) with lowest pH and clay contents over the soils CHI, BUN, GRÜ and BIB2 (29-36%) with acidic to intermediate pH to the soils HAU and SAR (0%) with lowest Zn contents. The results from LCF qualitatively matched the trends in Zn fractionation by sequential extraction (Fig. 6). While the exchangeable fraction F1 decreased with increasing soil pH, all soils contained a substantial percentage of Zn in the fractions F6+F7, which was highest in the soils HAU and SAR.

Even though all Zn–HIS references were included in the LCF analysis, the best fits were consistently obtained with the reference spectrum Zn–HIS-6.9-pH5. This reference is characterized by a relatively high Zn loading (Table 2) and a rather low Zn–Al coordination number (Table 4). Thus, the speciation of Zn within soil HIM was similar in all soils and indicative for a loading close to HIM sorption capacity. This interpretation is supported by estimates of the maximum amounts of soil Zn that can be retained by specific uptake into HIM (based on specific Zn adsorption maxima for HIS of 80 mmol/kg at pH 5.0 and 250 mmol/kg at pH 6.6, (Janssen et al., 2003b)). In a soil with pH 5.0 and a low clay content of 100 g/kg (assumed to consist of 25% HIM), the maximum soil Zn content sequestered into Zn–HIM would equal 131 mg/kg Zn, while 1020 mg/kg Zn could be specifically sorbed in HIM in a soil with pH 6.6 and 250 g/kg clay (assumed to consist of 25% HIM). Considering the Zn contents of the studied soils (Table 2), it is therefore likely that the HIM in most soils were loaded with Zn close to their sorption maximum.

Except for soil MOM, LCF also returned substantial fractions (13-48%) of Zn incorporated into phyllosilicates (using ZnMg-kerolites as proxies, Table 4). The fitted amounts of ZnMg-kerolite (fractions × soil Zn content) exceeded the upper limits for normal geogenic Zn contents in most soils. This suggests that the Zn-phyllosilicate formed in response to Zn input rather than being of geogenic origin, highlighting the relevance of these phases for Zn uptake in soils over wide pH ranges (Manceau et al., 2000; Nachtegaal et al., 2005a; Voegelin et al., 2005).

Previous studies reported the formation of Zn–HIM in contaminated and uncontaminated soils with pH 3.9–5.6 (Scheinost et al., 2002; Manceau et al., 2004; Manceau et al., 2005). In the present study, we identified Zn–HIM in a range of soils including soils with acidic pH as well as soils with slightly acidic to near-neutral pH containing inorganic C (GRÜ, BIB2, and HAU). These results demonstrate that formation of Zn–HIM is not restricted to acidic soil environments. Even though soil HAU had a neutral pH and contained substantial amounts of organic C, the major fraction of total Zn was associated with HIM, indicating the high stability of Zn–HIM even in environments where other Zn phases could form. In natural soils or soils contaminated with moderate amounts of Zn, incorporation of Zn into HIM may be a dominant sequestration pathway. However, the sorption capacity of HIM is limited. If continued Zn input into acidic soils leads to the accumulation of Zn to the sorption limits of HIM, further Zn will readily leach to deeper soil layers. In slightly acidic to neutral soils, on the other hand, saturation of HIM with Zn will result in Zn retention via alternative mechanisms such as enhanced Zn adsorption to soil organic matter or formation of Zn

bearing precipitates of the LDH- or phyllosilicate-type (Voegelin et al., 2005; Jacquat et al., 2008).

## 5. CONCLUSIONS

Zn sorption to Al-polymers in HIM at low loadings occurs in the dioctahedral vacancies of cyclic gibbsitic clusters. With increasing Zn loading, Zn sorption shifts to sites with decreasing Al coordination. Zn sorbed to the hydroxy-Al polymers in HIM are stable even under acidic conditions where other specific uptake mechanisms for Zn are less relevant. However, the sorption capacity of HIM is limited. Therefore, HIM may strongly affect the speciation of Zn in pristine soils or soils at moderate contamination levels, but do not allow to immobilize and accumulate continued input of high levels of Zn into soils.

## ACKNOWLEDGMENTS

Michel Schlegel and Darryl Roberts are acknowledged for providing several EXAFS spectra of reference compounds used in this study. We thank Farid Juillot for providing Zn-kaolinite samples, Beda Hofmann for providing natural Zn containing lithiophorite, Jakob Frommer for preparation of gibbsite, Gerome Tokpa for performing sequential extractions of soil samples, André Villard for thin section preparation and Kurt Barmettler and Charlotte Ganter for support in the laboratory. Three anonymous reviewers are thanked for their constructive comments on an earlier version of this manuscript. Stefan Mangold (XAS, ANKA, Germany) and Matthew Marcus (10.3.2, ALS, USA) are acknowledged for their help with data acquisition. The Angströmquelle Karlsruhe GmbH (ANKA, Karlsruhe, Germany) and the Advanced Light Source (ALS, Berkeley, USA) are acknowledged for providing beamtime. The ALS is supported by the Director, Office of Science, Office of Basic Energy Sciences, Material Sciences Division, of the U.S. Departement of Energy under Contract No. DE-AC03-76SF00098 at Lawrence Berkeley National Laboratory. This project was financially supported by the Swiss Science Foundation under Contract No. 200021-101876 and 200020-116592.

## APPENDIX A. SUPPLEMENTARY DATA

Supplementary data associated with this article can be found, in the online version, at doi:10.1016/j.gca.2008.10.026.

## REFERENCES

Ankudinov A. L., Ravel B., Rehr J. J. and Conradson S. D. (1998) Real-space multiple-scattering calculation and interpretation of x-ray-absorption near-edge structure. *Phys. Rev. B* **58**, 7565–7576.

Barnhisel R. I. and Bertsch P. M. (1989) Chlorites and hydroxy-interlayered vermiculite and smectite. In *Minerals in Soil Environments* (eds. J. B. Dixon and S. B. Weed). Soil Science Society of America, Madison.

Bish D. L. and Vondreele R. B. (1989) Rietveld refinement of non-hydrogen atomic positions in kaolinite. *Clays Clay Miner.* **37**, 289–296.

Bradbury M. H. and Baeyens B. (1998) $N_2$-BET surface area measurements on crushed and intact minerals and rocks: a proposal for estimating sorption transfer factors. *Nucl. Technol.* **122**, 250–253.

Brown G. and Farrow R. (1956) Introduction of glycerol into flakes aggregates by vapour pressure. *Clay Miner. Bull.* **3**, 44–45.

Brunton G. (1955) Vapor pressure glycolation of oriented clay minerals. *Am. Mineral.* **40**, 124–126.

Chao T. T. (1972) Selective dissolution of manganese oxides from soils and sediments with acidified hydroxylamine hydrochloride. *Soil Sci. Soc. Am. Proc.* **36**, 764–768.

Dixon J. B. and Jackson M. L. (1962) Properties of intergradient chlorite–expansible layer silicates of soil. *Soil Sci. Soc. Am. Proc.* **26**, 356–382.

Douglas L. A. (1989) Vermiculites. In *Minerals in Soil Environments* (eds. J. B. Dixon and S. B. Weed). Soil Science Society of America, Madison.

Elzinga E. J. and Reeder R. J. (2002) X-ray absorption spectroscopy study of $Cu^{2+}$ and $Zn^{2+}$ adsorption complexes at the calcite surface. Implications for site-specific metal incorporation preferences during calcite crystal growth. *Geochim. Cosmochim. Acta* **66**, 3943–3954.

Farmer V. C., Smith B. F. L., Wilson M. J., Loveland P. J. and Payton R. W. (1988) Readily-extractable hydroxyaluminium interlayers in clay- and silt-sized vermiculite. *Clay Miner.* **23**, 271–277.

Feng Q., Honbu C., Yanagisawa K. and Yamasaki N. (1999) Hydrothermal soft chemical reaction for formation of sandwich layered manganese oxide. *Chem. Mater.* **11**, 2444–2450.

Gee G. and Or D. (2002) Particle size analysis. In *Methods of Soil Analysis. Part 4: Physical Methods* (eds. J. H. Dane and C. C. Topp). Soil Science Society of America, Madison, USA.

Hendershot W. H. and Duquette M. (1986) A simple chloride method for determining cation exchange capacity and exchangeable cations. *Soil Sci. Soc. Am. J.* **50**, 605–608.

Isaure M.-P., Laboudigue A., Manceau A., Sarret G., Tiffrau C., Trocellier P., Lamble G. M., Hazemann J. L. and Chateigner D. (2002) Quantitative Zn speciation in a contaminated dredged sediment by μ-PIXE, μ-SXRF, EXAFS spectroscopy and principal component analysis. *Geochim. Cosmochim. Acta* **66**, 1549–1567.

Jacquat O., Voegelin A., Villard A., Marcus M. A. and Kretzschmar R. (2008) Formation of Zn-rich phyllosilicates, Zn-layered double hydroxide and hydrozincite in contaminated calcareous soils. *Geochim. Cosmochim. Acta* **72**, 5034–5057.

Janssen R. P. T., Bruggenwert M. G. M. and van Riemsdijk W. H. (2003a) Effect of Al hydroxide polymers on cation exchange of montmorillonite. *Eur. J. Soil Sci.* **54**, 335–345.

Janssen R. P. T., Bruggenwert M. G. M. and van Riemsdijk W. H. (2003b) Zinc ion adsorption on montmorillonite-Al hydroxide polymer systems. *Eur. J. Soil Sci.* **54**, 347–355.

Juillot F., Morin G., Ildefonse P., Calas G. and Brown G. E. (2006) EXAFS signature of structural Zn at trace levels in natural and synthetic trioctahedral 2:1 phyllosilicates. *Am. Mineral.* **91**, 1432–1441.

Keizer M. G. and Bruggenwert M. G. M. (1991) Adsorption of heavy metals by clay–aluminium hydroxide complexes. In *Interactions at the Soils Colloid–Soil Solution Interface* (eds. G. H. Bolt, M. F. De Boodt, M. H. B. Hayes and M. B. McBride). Kluwer Academic Publishers, Dordrecht.

Keller T. and Desaules A. (2001) *Böden der Schweiz: Schadstoffgehalte und Orientierungswerte. Umwelt Materialen 139, Bundesamt für Umwelt*. Wald and Lanschaft, Bern, Switzerland.

Kimpe C. R. (1993a) Clay and silt analysis. In *Soil Sampling and Methods of Analysis* (ed. M. R. Carter). Lewis Publishers, Boca Raton.

Kimpe C. R. (1993b) Soil separation for mineralogical analysis. In *Soil Sampling and Methods of Analysis* (ed. M. R. Carter). Lewis Publishers, Boca Raton.

Kirkland D. L. and Hajek B. F. (1972) Formula derivation of Al-interlayered vermiculite in selected soil clays. *Soil Sci.* **114**, 317–322.

Kyle J. H., Posner A. M. and Quirk J. P. (1975) Kinetics of isotopic exchange of phosphate adsorbed on gibbsite. *J. Soil Sci.* **26**, 32–43.

Lothenbach B., Furrer G. and Schulin R. (1997) Immobilization of heavy metals by polynuclear aluminium and montmorillonite compounds. *Environ. Sci. Technol.* **31**, 1452–1462.

Manceau A., Boisset M. C., Sarret G., Hazemann R. L., Mench M., Cambier P. and Prost R. (1996) Direct determination of lead speciation in contaminated soils by EXAFS spectroscopy. *Environ. Sci. Technol.* **30**, 1540–1552.

Manceau A. and Calas G. (1986) Nickel-bearing clay-minerals. 2. Intracrystalline distribution of nickel—an X-ray absorption study. *Clay Miner.* **21**, 341–360.

Manceau A., Lanson B., Schlegel M. L., Harge J. C., Musso M., Eybert-Berard L., Hazemann J. L., Chateigner D. and Lamble G. M. (2000) Quantitative Zn speciation in smelter-contaminated soils by EXAFS spectroscopy. *Am. J. Sci.* **300**, 289–343.

Manceau A., Marcus M. A., Tamura N., Proux O., Geoffroy N. and Lanson B. (2004) Natural speciation of Zn at the micrometer scale in a clayey soil using X-ray fluorescence, absorption, and diffraction. *Geochim. Cosmochim. Acta* **68**, 2467–2483.

Manceau A., Tamura N., Celestre R. S., MacDowell A. A., Geoffroy N., Sposito G. and Padmore H. A. (2003) Molecular-scale speciation of Zn and Ni in soil ferromanganese nodules from loess soils of the Mississippi Basin. *Environ. Sci. Technol.* **37**, 75–80.

Manceau A., Tommaseo C., Rihs S., Geoffroy N., Chateigner D., Schlegel M. L., Tisserand D., Marcus M. A., Tamura N. and Zueng-Sang C. (2005) Natural speciation of Mn, Ni, and Zn at the micrometer scale in a clayey paddy soil using X-ray fluorescence, absorption, and diffraction. *Geochim. Cosmochim. Acta* **60**, 3034–4007.

Marcus M. A., MacDowell A. A., Celestre R. S., Manceau A., Miler T., Padmore H. A. and Sublett R. E. (2004) Beamline 10.3.2 at ALS: a hard X-ray microprobe for environmental and materials science. *J. Synchrotron Radiat.* **11**, 239–247.

Meunier A. (2007) Soil hydroxy-interlayered minerals: A re-interpretation of their crystallochemical properties. *Clays Clay Miner.* **55**, 380–388.

Nachtegaal M., Marcus M. A., Sonke J. E., Vangronsveld J., Livi K. J. T., Van der Lelie D. and Sparks D. L. (2005a) Effects of in situ remediation on the speciation and bioavailability of zinc in a smelter contaminated soil. *Geochim. Cosmochim. Acta* **69**, 4649–4664.

Nachtegaal M., Scheidegger A. M., Dahn R., Chateigner D. and Furrer G. (2005b) Immobilization of Ni by Al-modified montmorillonite: a novel uptake mechanism. *Geochim. Cosmochim. Acta* **69**, 4211–4225.

O'Day P., Rehr J. J., Zabinsky S. I. and Brown G. E. J. (1994) Extended X-ray absorption fine structure (EXAFS) analysis of disorder and multiple-scattering in complex crystalline solids. *J. Am. Chem. Soc.* **116**, 2938–2949.

Odnevall Wallinder I., Leygraf C., Karlèn C., Heijerick D. G. and Janssen C. R. (2001) Atmospheric corrosion of zinc-based materials runoff rates, chemical speciation and ecotoxicity effects. *Corros. Sci.* **43**, 809–816.

Perdikatsis B. and Burzlaff H. (1981) Structural refinement of talc $Mg_3[(OH)_2Si_4O_{10}]$. *Z. Kristallogr.* **156**, 177–186.

Petit S., Decarreau A., Mosser C., Ehret G. and Grauby O. (1995) Hydrothermal synthesis (250 °C) of copper-substituted kaolinites. *Clays Clay Miner.* **43**, 482–494.

Ravel B. (2001) ATOMS: crystallography for the X-ray absorption spectroscopist. *J. Synchrotron Radiat.* **8**, 314–316.

Ravel B. and Newville M. (2005) Athena, Artemis, Hephaestus: data analysis for X-ray absorption spectroscopy using IFEFFIT. *J. Synchrotron Radiat.* **12**, 537–541.

Rich C. I. (1968) Hydroxy interlayers in expansible layer silicates. *Clays Clay Miner.* **16**, 15–30.

Roberts D. R., Ford R. G. and Sparks D. L. (2003) Kinetics and mechanisms of Zn complexation on metal oxides using EXAFS spectroscopy. *J. Colloid Interface Sci.* **263**, 364–376.

Saalfeld H. and Wedde M. (1974) Refinement of crystal-structure of gibbsite, $Al(OH)_3$. *Z. Kristallogr.* **139**, 129–135.

Saha U. K., Taniguchi S. and Sakurai K. (2001) Adsorption behavior of cadmium, zinc, and lead on hydroxyaluminum– and hydroxyaluminosilicate–montmorillonite complexes. *Soil Sci. Soc. Am. J.* **65**, 694–703.

Sarret G., Saumitou-Laprade P., Bert V., Proux O., Hazemann J. L., Traverse A., Marcus M. A. and Manceau A. (2002) Forms of zinc accumulated in the hyperaccumulator *Arabidopsis halleri*. *Plant Physiol.* **130**, 1815–1826.

Scheinost A. C., Kretzschmar R., Pfister S. and Roberts D. R. (2002) Combining selective sequential extractions, X-ray absorption spectroscopy, and principal component analysis for quantitative zinc speciation in soil. *Environ. Sci. Technol.* **36**, 5021–5028.

Schlegel M. L. and Manceau A. (2006) Evidence for the nucleation and epitaxial growth of Zn phyllosilicate on montmorillonite. *Geochim. Cosmochim. Acta* **70**, 901–917.

Schlegel M. L. and Manceau A. (2007) Zn incorporation in hydroxy-Al- and Keggin Al-13-intercalated montmorillonite: a powder and polarized EXAFS study. *Environ. Sci. Technol.* **41**, 1942–1948.

Schlegel M. L., Manceau A. and Charlet L. (1997) EXAFS study of Zn and ZnEDTA sorption at the goethite (alpha-FeOOH)/water interface. *J. Phys. IV* **7**, 823–824.

Tamura T. (1958) Identification of clay minerals from acid soils. *J. Soil Sci.* **9**, 141–147.

Teo B. K. (1986) *EXAFS: Basic Principles and Data Analysis*. Springer, Berlin.

van Olphen H. and Fripiat J. J. (1979) *Data Handbook for Clay Minerals and Other Non-Metallic Minerals*. Pergamon Press, Oxford.

Voegelin A., Pfister S., Scheinost A. C., Marcus M. A. and Kretzschmar R. (2005) Changes in zinc speciation in field soil after contamination with zinc oxide. *Environ. Sci. Technol.* **39**, 6616–6623.

Voegelin A., Tokpa G., Jacquat O., Barmettler K. and Kretzschmar R. (2008) Zinc fractionation in contaminated soils by sequential and single extractions: influence of soil properties and zinc content. *J. Environ. Qual.* **37**, 1190–1200.

Zeien H. and Brümmer G. W. (1989) Chemische Extraktionen zur Bestimmung von Schwermetallbindungsformen in Böden. *Mitt. Dtsch. Bodenkundl. Ges.* **59**, 505–510.

*Associate editor:* Donald L. Sparks